

Three-Dimensional Simulations of Stratospheric N₂O: Predictions for Other Trace Constituents

J. D. MAHLMAN, H. LEVY II, AND W. J. MOXIM

Geophysical Fluid Dynamics Laboratory, Princeton University, Princeton, New Jersey

The Geophysical Fluid Dynamics Laboratory (GFDL) three-dimensional general circulation/tracer model has been used to investigate the stratospheric behavior of N₂O under a range of photodestruction hypotheses. A comparison of observations with these simulations shows that the atmospheric N₂O lifetime lies between 100 and 130 years. For the three experiments conducted, it was found that the model-derived global one-dimensional eddy diffusion coefficients K_z for one experiment are appropriate for the other two experiments as well. In addition, the meridional slopes of N₂O mixing ratio isolines are virtually identical in the lower stratosphere for all three experiments. The generality of these two results was explored with a simple "two-slab" model. In this model the equilibrium meridional slopes of trace gas isolines and K_z values are solved directly. The model predicts that long-lived gases with weak photodestruction rates should have similar meridional slopes, but the effect of faster destruction is to flatten the meridional slopes. The simple model also predicts that K_z depends upon chemical processes through a direct dependence upon the meridional slope for a given gas as well as upon the intensity with which upward propagating tropospheric disturbances force the stratospheric zonal winds. The three N₂O experiments have been compared against detailed observational analyses. These analyses show that the model meridional N₂O slopes are too flat by about 30%. The simple two-slab model indicates that this results from a somewhat weak forcing of the model stratospheric zonal winds. A comparison of the temporal variability of model N₂O against the "Δ" statistics of Ehhalt et al. (1983) shows good agreement. Another simple theoretical model is proposed that shows why Δ statistics are so useful and predicts the circumstances under which different destruction chemistries should lead to different Δ statistics. These results have allowed a very general extrapolation of the three N₂O numerical experiments to predicted structure for a wide class of long-lived trace gases. Specifically, the supporting theoretical developments allow predictions for the effect of chemistry on the global (one-dimensional) behavior, meridional-height (two-dimensional) structure, and local temporal variability. Finally, some examples of transient behavior are presented through model time series at points corresponding to available measurements. These time series, with the support of horizontal N₂O charts, show complex behavior, including pronounced seasonal cycles, transport-produced N₂O "inversions," and detailed meridional transport events associated with transient stratospheric disturbances.

1. INTRODUCTION

An understanding of atmospheric N₂O is of great interest because of its fundamental role in the budget of stratospheric ozone. N₂O is produced in the lower troposphere by various processes (for a review and relevant literature, see *Levy and Mahlman* [1980] and *McElroy* [1980]). It eventually is transported to the middle stratosphere, where it is destroyed by photodissociation and by reaction with O(¹D).

N₂O is also of special concern because of its rather close similarity to a large class of long-lived gases with sources in the troposphere and photodestruction-related sinks in the stratosphere. Most notable among these are N₂O, CH₄, CF₂Cl₂, and CFCI₃ because of their direct and indirect effects on ozone as well as their contributions to the climate greenhouse effect. Thus a proper simulation and understanding of the behavior of N₂O may be regarded as a key to understanding the behavior and influence of a wider variety of long-lived trace gasses.

It is the three components of production, transport, and destruction which must be properly accounted for in a successful simulation of N₂O. In 1976 we began to study this problem through use of the GFDL three-dimensional general circulation/tracer model [*Mahlman and Moxim*, 1978]. At that time virtually nothing was known about the tropospheric sources of N₂O, while the observed "climatology" of N₂O was extremely uncertain.

Accordingly, we designed an experiment which built upon

the best available information. First, we assumed that current methodology was sufficient to calculate the stratospheric destruction of N₂O. Then, we assumed that the tropospheric mixing ratio of N₂O was a value of about 295 parts per billion by volume (ppbv) (halfway between the "observed" extremes of 260–330 ppbv at that time). The consistent global mean surface source strength was then estimated iteratively to be about 1.3×10^9 molecules cm⁻² s⁻¹. Some results of that experiment are given by *Levy et al.* [1979]. The parts of that work applicable to the stratosphere will be reviewed later in this paper. Generally, however, the stratospheric N₂O simulation in that experiment showed encouraging agreement with available observations.

Using this framework, a series of experiments was conducted to investigate the impact of possible surface N₂O source distributions on the tropospheric N₂O structure. Results from those experiments are available in work by *Levy and Mahlman* [1980] and *Levy et al.* [1982]. For this study, which emphasizes the stratosphere, the important result of those experiments is that the stratospheric model N₂O structure is almost completely independent of the surface N₂O source distribution. Thus the remaining uncertainties concerning the nature of the surface N₂O source need not concern us here.

After our first N₂O experiment was completed we learned that improved measurements of the photodissociation of N₂O (including temperature dependence) had been reported by *Selwyn et al.* [1977]. These newer measurements indicated generally slower destruction rates for stratospheric N₂O. In response to this we decided to design a new N₂O model experiment which incorporated the newer photodissociation cross sections. The results and implications of that experiment are analyzed here.

This paper is not subject to U.S. copyright. Published in 1986 by the American Geophysical Union.

Paper number 5D0862.

As shall later become clear, the above "correct" experiment (which we will designate "Slow-Sink" N₂O) reveals a large sensitivity of the results to the effective stratospheric N₂O destruction rate. This led us to design a third experiment which helps explore this sensitivity. Here we have examined the impact of more rapid destruction rates by arbitrarily doubling the removal coefficients in the control ("Uniform Source" N₂O) experiment. This "Fast-Sink" N₂O experiment thus allows us to examine the effect of a reasonably wide range of stratospheric destruction rates on the three-dimensional distribution of long-lived trace gases. These experiments thus may be applicable to gases with overall characteristics similar to N₂O.

A major goal of this work is to seek a generalized understanding of the impact of chemical destruction on the transport and distribution of a wide class of long-lived trace gases. In the first three sections we will begin by examining the three N₂O numerical experiments and their relation to each other as well as to available observations. The generality of the model behavior and its dependence on chemical processes will be examined through a companion theoretical development described in section 4, used in section 5, and developed in detail in the appendix.

In section 6 the simulated variability of N₂O and its relationship to available observations will be addressed. Finally, theoretical insights developed in section 4 are used to develop a diagnosis of the expected role of chemical processes in understanding the temporal variability of various trace gases.

This sequence of developments will provide a unifying perspective on the generalized interpretation of observed and simulated trace gas behavior for a wide range of source and sink chemistries. Accordingly, this work should prove useful in the design and interpretation of numerical trace constituent models in one, two, and three dimensions.

2. DESIGN OF N₂O EXPERIMENTS

2.1. "Regular-Sink" N₂O

This experiment is the same as the "Uniform Source" integration described by *Levy et al.* [1979, 1982]. (The nomenclature has been changed here because it is only the stratospheric destruction characteristics that are relevant in the set of experiments reported here.) The surface source is uniform over the globe, with its final magnitude being determined iteratively so as to give a tropospheric mixing ratio of about 295 ppbv and to balance the stratospheric destruction calculation as described in the work by *Levy et al.* cited above.

This experiment has been run through 7½ annual cycles. By using the reinitialization technique described by *Levy et al.* [1982] the end of the integration has been determined to be less than 0.3% below the equilibrium value at any point in the model atmosphere. The surface source strength corresponding to a final "best estimate" of N₂O equilibrium is 1.442×10^9 molecules cm⁻² s⁻¹. This value is nearly 11% higher than the estimate of 1.3×10^9 molecules cm⁻² s⁻¹ described in the preliminary report of *Levy et al.* [1979] after a few years of model integration. The model-determined global mean "residence time" corresponding to this source is 131.2 years.

2.2. "Slow-Sink" N₂O

In this experiment the global uniformity of the surface source, the strategy for obtaining its self-consistent magnitude, and the tropospheric N₂O mixing ratio are all the same as in the Regular-Sink N₂O experiment. The calculation of stratospheric N₂O destruction is the same as described by *Levy et al.* [1982], with the following exceptions: we use the

temperature-dependent N₂O absorption cross-section values of *Selwyn et al.* [1977]; the temperature-dependent form of the O(¹D) quantum yield [*Moortgat and Kudzus*, 1978] are used with an upper limit of 0.88 rather than 1.0; updated O(¹D) reaction rate coefficients are taken from the compilation by *Hampson* [1980]; and the revised solar flux data of *Simon* [1978] replace that of *Ackerman* [1971].

To save computer resources, a "good guess" initial condition for this experiment was determined in the following manner. First, a one-dimensional model was utilized which is designed to provide a self-consistent subset of the three-dimensional model in terms of model levels, computational algorithms, etc. The one-dimensional vertical eddy diffusion coefficients K_z were calculated from the three-dimensional model's annual mean vertical transport for Regular-Sink N₂O. The one-dimensional model was then set up to reproduce the height-dependent, horizontal, averaged N₂O mixing ratio obtained in the regular-sink experiment.

Once this one-dimensional model of N₂O could reproduce the three-dimensional horizontally averaged profile for Regular-Sink, the revised Slow-Sink destruction parameterization described above was inserted into the one-dimensional model, followed by a 2000-year integration to the new equilibrium. The one-dimensional source strength was then scaled to bring the one-dimensional tropospheric mixing ratios into agreement for both the Regular-Sink and Slow-Sink N₂O experiments.

The initial field for the Slow-Sink three-dimensional integration was constructed on each model isobaric surface through multiplication of the three-dimensional regular-sink N₂O field by the ratio (Slow-Sink/Regular-Sink) of the one-dimensional mixing ratios at the appropriate pressure levels. The new three-dimensional surface source was initially set to equal the stratospheric sink determined from the one-dimensional Slow-Sink experiment.

Even though much of the adjustment to the revised stratospheric destruction rates is three-dimensional, we found this initial condition shortened the required integration time considerably by starting with a reasonable one-dimensional profile. This was the case even though the horizontal N₂O gradients corresponded to those of the previous experiment.

This Slow-Sink N₂O experiment was run for 3 years. We found that very little further adjustment of the vertical N₂O profile was required to obtain a result satisfactorily close to the final equilibrium solution. This implies that one-dimensional eddy diffusion coefficients determined self consistently for a given long-lived trace constituent (Regular-Sink) may be applicable to the one-dimensional transport of other sufficiently long-lived constituents. This of course requires that the chemical destruction is modeled properly for both constituents. Otherwise, the derived coefficients would implicitly contain effects other than horizontally averaged vertical transport. However, the theoretical development in the appendix will show circumstances under which this alleged "universality" of K_z is no longer true.

At the end of the 3-year integration of Slow-Sink N₂O, the solution has been determined to be at most 0.15% below the equilibrium value everywhere in the model domain. The estimates of the degree of departure from final equilibrium are determined by the "shooting" to equilibrium method described by *Levy et al.* [1982, equation (6)]. The surface source strength corresponding to the final "best estimate" of N₂O equilibrium is 1.056×10^9 molecules cm⁻² s⁻¹. The model global mean residence time corresponding to this source is 180.2 years.

It should be pointed out that in calculating behavior of such

long-lived trace constituents we have to be especially mindful of global conservation properties. For example, an N₂O mass loss of 0.5% per year due to computer round off error or coding inconsistencies would be as large in magnitude as the Slow-Sink N₂O destruction itself. In this model, care has been taken to insure that the mass change due to machine round off is always 2 to 3 orders of magnitude smaller than that of the net source or sink.

2.3. "Fast-Sink" N₂O

The basic design and strategy for this Fast-Sink N₂O experiment is the same as described above for the previous two experiments. The only difference is that the N₂O removal coefficients derived for the Regular-Sink N₂O experiment have been doubled. This choice has no direct physical justification other than to evaluate the model's sensitivity to faster destruction rates than those of the first two experiments. This allows us to explore the applicability of the insights gained here to other long-lived trace gases. Also, it allows consideration of the possibility that N₂O might be experiencing faster stratospheric destruction than implied at the current level of knowledge.

This Fast-Sink N₂O experiment has been run for 3½ years and has been determined to be everywhere less than 0.1% below the final equilibrium value. There is no special significance to the fact that all three experiments were terminated at values slightly smaller than their "true equilibrium" values. The surface source strength corresponding to the final "best estimate" of equilibrium for the Fast-Sink N₂O experiment is 1.965×10^9 molecules cm⁻² s⁻¹. This source corresponds to a model residence time of 96.3 years.

3. TIME MEAN BEHAVIOR

3.1. Comparison of Experiments

In comparing the behavior of the three N₂O model experiments we first concentrate on the zonal mean structure. Figure 1 shows cross sections of zonal mean N₂O mixing ratio from the Fast-Sink and Slow-Sink experiment for the months of January, April, July, and October as well as the January and July fields for the Slow-Sink experiment. The Regular-Sink experiment is not shown because its structure is midway between these extremes.

Many of the results displayed in Figure 1 show the same features already noted by *Levy et al.* [1979]: the upward equatorial bulge; pronounced meridional slopes of isolines, with steeper slopes present in the northern hemisphere at every comparable season; and pronounced downward depressions of lower values in the winter higher latitudes. In April and October the downward depressions show clearly the "lag" effect of the winter season in each hemisphere. Note also that the equatorial bulge shows some tendency to follow the sun's overhead position with some seasonal lag.

In the lower stratosphere and upper troposphere, Figure 1 shows a pronounced interhemispheric asymmetry, with smaller northern hemisphere than southern hemisphere values at corresponding latitudes during every month. This asymmetry was noted earlier in the tropospheric N₂O study by *Levy et al.* [1982]. The explanation for this effect appears to be related to a surprising, but understandable, model phenomenon. Dynamical analysis of this model [*Manabe and Mahlman, 1976*] shows a significantly higher eddy activity in the northern hemisphere stratosphere in comparison to the southern hemisphere. Associated with this extra eddy activity is a larger departure from radiative equilibrium and a net stratospheric radiative cooling in the northern hemisphere over the

annual cycle. This cooling is balanced by a very weak interhemispheric meridional circulation with hemispheric averaged vertical velocities of ~ 3 km yr⁻¹ (~ 0.01 cm s⁻¹) (sinking in northern hemisphere). This differential mean vertical velocity of 6 km yr⁻¹ is sufficient to explain the model's interhemispheric N₂O asymmetry. It remains to be determined whether or not this degree of asymmetry is present in the real atmosphere.

A comparison of the Fast-Sink against the Slow-Sink N₂O fields in Figure 1 shows a very significant difference in the vertical gradients of N₂O, with weaker gradients being associated with weaker destruction (Slow-Sink). Comparison of the 10 mbar meridional variations of N₂O shows the strongest gradients in Fast-Sink N₂O. Its annual average north polar value is 68 ppbv, and the corresponding equatorial value is 141. In Slow-Sink N₂O the north polar and equatorial annual mean 10 mbar values are 153 and 205 ppbv, respectively.

The above results indicate that a change in vertical gradient is associated with a concomitant change in horizontal gradient. This is visually obvious in Figure 1 by noting that the meridional slopes of the R_{N₂O} surfaces are virtually unchanged over the two experiments shown at any given time of year. This observation, when combined with the predictable one-dimensional behavior already noted in sections 2.1 and 2.2, provides a means of predicting the behavior of a wide class of long-lived trace constituents independent of the magnitude of their vertical mixing ratio gradients. That is, if the nature of the stratospheric destruction (or production) is known, the global average vertical profile can be predicted with some accuracy using a simple one-dimensional model. Once this is known, the above information on the generalized meridional slopes of trace constituent isolines might be used to predict the latitude-height distribution (in principle, at least) for the zonal mean mixing ratio of the constituent of interest.

This prediction can be evaluated if real data is present in sufficient quantities. It is also possible that this approach can be used to evaluate possible measurement inaccuracies in the "observed" data set for similar trace constituents. We will address this in the next section.

The apparent validity of these relationships lends some support to the one-dimensional modeling approach of *Wofsy* [1976] in which the global model mixing ratios are spread out along "mixing surfaces," paralleling the observed tracer meridional slopes. However, a careful analysis shows that such slopes cannot be regarded as "mixing surfaces" but rather appear as a balance among competitive processes [see *Mahlman et al.*, 1980, 1984]. Nevertheless, such a procedure could prove to be empirically useful, irrespective of the physical processes responsible for producing the equilibrium slopes.

As with most "general" relationships, there are limits to the useful range of application. It should not be expected to apply for a trace constituent which is far from its transport-chemical equilibrium. See, for example, the early evolution of the "Instantaneous Source" experiment of *Mahlman and Moxim* [1978, Figure 5.1a]. Further, it should not apply for a trace constituent in which the production or destruction time scales are of comparable order (or shorter) to the time required for meridional or vertical exchange. An instructive example can be found in Figure 3.3 of *Mahlman et al.* [1980]. In the lower stratosphere the meridional slopes of ozone in that experiment are very similar to the N₂O slopes seen here in Figure 1. This is because the chemical sources and sinks are essentially zero there for both modeled constituents. However, in the middle stratosphere the ozone isoline slopes are totally unlike the N₂O slopes because the ozone production-destruction time scale is much faster than that of N₂O destruction. In fact, the

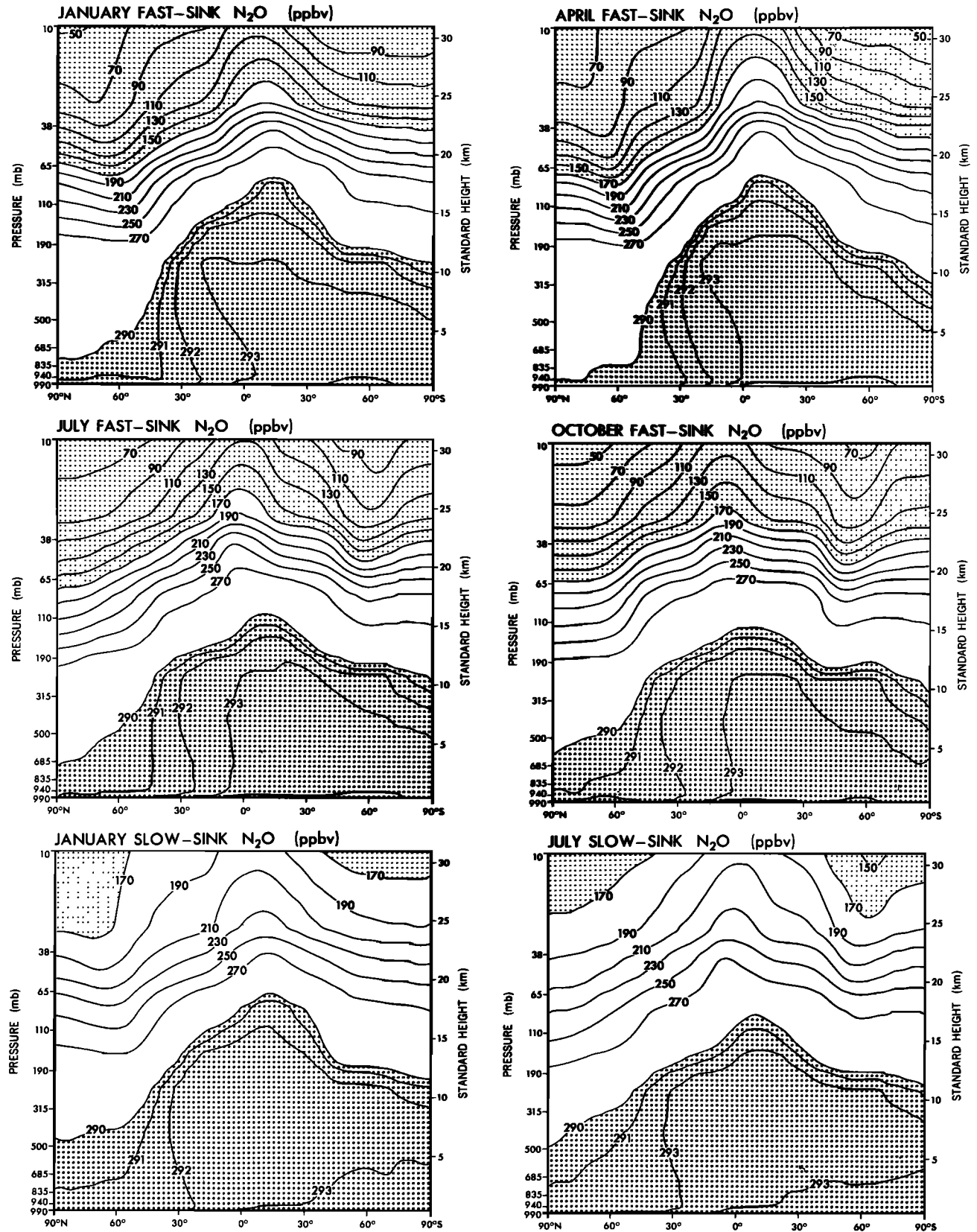


Fig. 1. Zonal mean N₂O mixing ratio (ppbv) for January, April, July, and October for the Fast-Sink experiment and January and July for the Slow-Sink model experiment.

N₂O destruction is always so weak that midstratospheric mixing ratios are largest in the tropics, where the destruction rate is the fastest. We note that these chemical circumstances which break the “constant slope” result are essentially the same as those qualitatively demonstrated by *Mahlman* [1975] to lead to species-dependent effective one-dimensional eddy diffusion coefficients for various modeled trace constituents. We have not yet established, however, how slow the chemical destruction must be to retain the validity of this “constant slope” result. This question is examined carefully in section 4 and the appendix.

An additional examination of the model experiments shows that the above result can be generalized to three dimensions. The topography of surfaces of the time-averaged mixing ratio is essentially the same for all similarly long-lived trace constituents. This means that the local meridional and longitudinal slopes of time mean mixing ratio surfaces tend to be the same for trace substances in transport/chemical equilibrium as long as their source-sink chemistries are similar or are weak relative to transport. This property will prove useful for the analysis of N₂O variability presented in sections 6 and 7.

3.2. Comparison With Observations

It is fortunate for this study that detailed measurements of long-lived species have been conducted by the National Oceanic and Atmospheric Administration (NOAA) Aeronomy Laboratory scientists at some selected geographical sites [*Schmeltekopf et al.*, 1977; *Goldan et al.*, 1980]. Partly in support of the present study, these data have been analyzed in greater detail by J. T. Bacmeister et al. (unpublished manuscript, 1986) (hereafter referred to as BAM86). The measurements obtained include the chlorofluorocarbons CCl₃F and CCl₂F₂ in addition to N₂O. This provides an opportunity to evaluate some of the “tracer slope” model results of the previous section.

Figure 2 shows the BAM86 annual mean N₂O mixing ratio (in ppbv) at Laramie, Wyoming (41°N, 105°W). Also shown are annual mean vertical profiles for the “Laramie” location from the three model experiments described in section 2. Note that the observed profile agrees closest with the Fast-Sink N₂O experiment. Recall that the Slow-Sink N₂O experiment is the one designed to reflect the best calculation of N₂O destruction as of 1980. This destruction rate appears to be much too slow. Furthermore, recent observations of solar flux in the middle

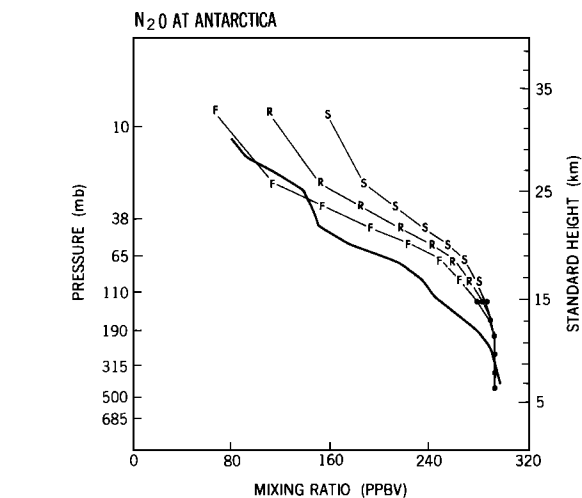


Fig. 3. Same as Figure 2, except at Antarctica (80°S, 120°W).

stratosphere [*Frederick and Mentall*, 1982] support a faster destruction rate than used in Slow-Sink N₂O.

Given in Figure 3 are the summer (December-January-February) profiles of N₂O at Antarctica (80°S, 120°W) (BAM86) and the model results for the three experiments at the same location and time interval. Again, the observed profile is most like that of the Fast-Sink N₂O experiment. Note that the Antarctica mixing ratio decrease with altitude is rather similar to that of Laramie in Figure 2 for both model and observations.

Figure 4 shows the BAM86 combined averages for the Canal Zone (9°N, 80°W) and Brazil (5°S, 38°W). Here the samples were combined to enhance statistical significance. The three model experiments shown are from the model grid point encompassing the Canal Zone location. In this figure the observed profile is closest to that of Regular-Sink N₂O.

While the “best” calculation of N₂O as of 1980 is clearly too slow, all the discrepancies cannot be explained away by a judicious choice of the N₂O removal efficiency in the three-dimensional model. Rather, for a given choice of tropical profile it is clear that the higher-latitude points of the model do not decrease with altitude rapidly enough. From another perspective the meridional slopes of the mean isolines of R_{N₂O} are not as steep in the model (see Figure 1) as they are in the

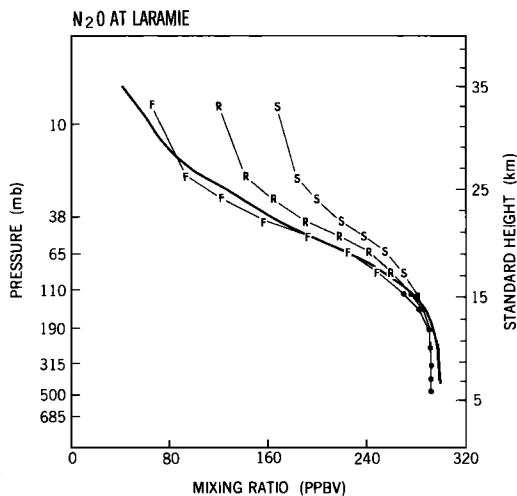


Fig. 2. Annual mean N₂O mixing ratio (ppbv) profile at Laramie, Wyoming (41°N, 105°W) from BAM86 (heavy line). Also shown are model annual mean N₂O profiles for the “Laramie” location from the Fast-Sink (F), Regular-Sink (R), and Slow-Sink (S) N₂O experiments.

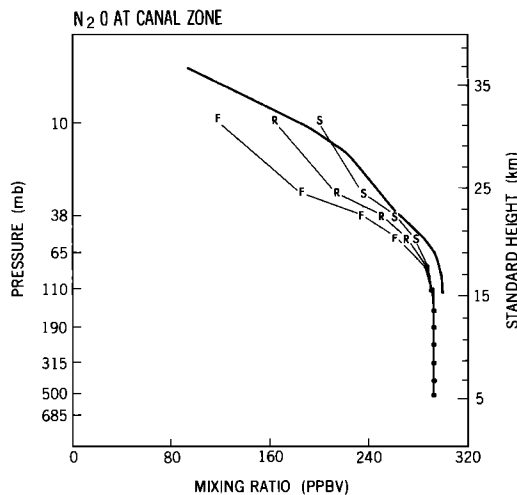


Fig. 4. Same as Figure 2, except at average of Canal Zone (9°N, 80°W) and Brazil (5°S, 38°W).

observations. Roughly, the data suggest that the hemispheric mean observed meridional slopes are perhaps 30% steeper than those simulated by the model.

This result showing a model deficiency is surprisingly clear considering the severe geographical and temporal limitations of the observed data. The difference in slope shows up in the BAM86 CF₂Cl₂ data as well. This is a good example of how useful local data sets can be for three-dimensional model evaluation. Discussion on the probable cause of this modeling discrepancy is given in section 5.

4. THEORETICAL INTERPRETATION OF MERIDIONAL TRACER SLOPES

The simulated results showing strong similarities among the meridional slopes of N₂O isolines for the three experiments leads us to pursue a more quantitative diagnosis of such behavior. In particular, we wish to examine the role of chemical destruction processes relative to that of dynamical mechanisms in determining meridional trace constituent slopes.

Briefly restated, the model experiments indicate that for sufficiently weak photodestruction chemistries, the spatial slopes of the time mean equilibrium mixing ratio isolines are essentially the same for all such long-lived trace constituents. The data of BAM86 shows clearly that this result is verified in the comparison of N₂O and CF₂Cl₂ slopes. However, the slopes of CFCl₃ are significantly flatter than those for N₂O and CF₂Cl₂. This implies that the destruction rate of CFCl₃ is sufficiently fast so as to impede the net dynamical tendency to establish similar time mean slopes for vertically stratified tracers.

How fast is sufficiently fast? In an attempt to answer this in a straightforward way, a simple "two-slab" model is developed in the appendix. The simple model distills the insights offered by *Mahlman et al.* [1984], *Mahlman* [1985], and *Plumb and Mahlman* [1986] on the essential processes governing the observed poleward-downward slopes of mean mixing ratio isolines in the lower stratosphere.

To a very crude approximation those results indicate that the two-dimensional equilibrium slope exists as a balance between zonal mean advection by the "diabatic" circulation and an effective meridional diffusion. This balance is used as a basis for the governing equation to develop the two-slab model. It is given as equation (A1) in the appendix, along with more complete descriptions.

The use of the two-slab approximation (dividing the hemisphere into two equal area boxes) allows a straightforward solution to the simplified equations: a meridional structure (slope) part and a vertical structure of the horizontal average part (one-dimensional behavior). As demonstrated in the appendix, each of these solutions depends upon the nature of chemical processes in a readily understandable fashion.

We must point out here that this two-dimensional model should not be interpreted as a viable substitute for more complete two-dimensional transport parameterizations such as that given by *Plumb and Mahlman* [1986]. Rather, the goal is to isolate mechanisms determining the impact of chemical destruction processes on the global distribution of long-lived trace gases. A bonus from this analysis is that the relationship between one-dimensional and two-dimensional models is significantly clarified.

Because of the mathematical complexity of the analysis, the details of the two-slab model and its accompanying physical insights are presented in the appendix. The reader uninterested in such details can skip the appendix and still examine the major implications of that development in the following two

paragraphs. For details and their implications for understanding one-dimensional and two-dimensional transport models, refer directly to the appendix.

The two-slab model of the appendix shows that the equilibrium poleward-downward slopes of mixing ratio isolines depend importantly on the photodestruction efficiency. Equation (A36) shows that as the destruction efficiency increases, the meridional slope ($\partial z/\partial y_R$) flattens. However, for longer destruction times (inverse of destruction coefficient) greater than, say, 700 days, the meridional slopes are essentially independent of chemistry (see Figure A1). This result suggests that the slope prediction of Figure A1 can be tested against the results of the Fast-Sink and Slow-Sink N₂O experiments. For the Fast-Sink experiment the tropical destruction rate $\langle C \rangle^T$ at 10 mbar is about $3.9 \times 10^{-8} \text{ s}^{-1}$ (≈ 297 days). ($\langle C \rangle^T$ is the destruction parameter appearing in the slope equation (A36)). For the Slow-Sink N₂O experiment, $\langle C \rangle^T$ is about $1.16 \times 10^{-8} \text{ s}^{-1}$ (≈ 1000 days). The two-slab model results shown in Figure A1 predict 10-mbar meridional slopes of -0.665×10^{-3} and -0.855×10^{-3} , respectively, for a difference of about 22%. Comparisons of the actual slopes near 10 mbar for these two three-dimensional experiments show differences ranging from ~ 15 –25%. Thus this two-dimensional mechanistic model appears to capture the effect of faster chemistry on the three-dimensional model's meridional slopes. These predictions should be tested more carefully against available data and against three-dimensional model experiments using faster destruction rates, such as those for CFCl₃.

The second major conclusion of the appendix is that the effective global average eddy diffusion coefficient K_z depends indirectly upon the photodestruction coefficient in a predictable way (see Figure A1). In particular, equation (A32) shows that K_z depends directly upon the magnitude of the meridional slope ($\partial z/\partial y_R$). A plot of the predicted dependence of K_z on the tropical photodestruction rate is given in Figure A1. Thus in the two-slab model the effect of faster destruction chemistries is to slow down the global mean vertical tracer flux for a given mean gradient. How this variable K_z effect could change the ozone photochemical predictions for global one-dimensional models remains to be determined.

Both major conclusions gained from the two-slab model of the appendix thus refute the tentative implications of sections 2 and 3. Instead, (A32) and (A36) show the apparent "universality" of the meridional slopes and one-dimensional K_z s to be true only for rather slow destruction chemistries. The effect of faster chemistries is to flatten the meridional slope and therefore to reduce the effective one-dimensional K_z value.

5. CAUSE OF THE "FLATTENED SLOPE" MODEL DISCREPANCY

In section 3 it was shown that the meridional slopes of N₂O isolines in the three-dimensional experiment were too flat by $\sim 30\%$ in comparison with available observations from BAM86. For understanding the biases of this model, as well as for designing future models, it is of interest to try to understand the cause of this discrepancy. The insights gained in section 4 and the appendix allow such an assessment.

The simple two-slab model given in the appendix suggests that the only significant mechanism leading to a slope-steepening effect is that of the diabatic (or similar) meridional circulation. Thus in the context of that simple model the three-dimensional model apparently needs a stronger meridional gradient of diabatic heating (more tropical heating and polar cooling).

This prediction is quite compatible with a well-known bias

of this general circulation model (GCM) (e.g., see *Manabe and Mahlman* [1976]). The model polar regions (except summer) are significantly too cold relative to observations. Thus one can readily conclude that the model temperature fields are too close to their radiative equilibrium values [see *Mahlman and Umscheid*, 1984]; therefore the magnitude of the model's meridional gradient of net diabatic heating is indeed too weak.

This is simply another verification of the often underappreciated fact that the annual mean net diabatic heating of the stratosphere must ultimately be due to dynamical processes [Fels et al., 1980]. This perspective is compatible with the "transformed Eulerian" mean framework of *Andrews and McIntyre* [1976]. As shown, for example, by *Andrews et al.* [1983, equation (B13)], the role of tropospheric disturbances propagating into the stratosphere is to produce a convergence of "Eliassen-Palm flux," a measure of the net decelerative force produced by nonzonal disturbances. The decelerative effect produced by this zonal force acts to excite a "residual" circulation (which is qualitatively similar to the diabatic circulation), manifested by rising motion (and adiabatic cooling) in lower latitudes and sinking motion (and adiabatic heating) in higher latitudes. This high-latitude dynamical heating is balanced in the annual mean by net radiative cooling. Thus the stratosphere can be thought of as being driven from radiative equilibrium by the dissipation of tropospheric disturbances propagating into the stratosphere. Without such disturbances, the system would be very close to radiative equilibrium, with accompanying small values of net diabatic heating.

In the context of the transport discrepancy found in the three-dimensional model it can be concluded that the magnitude of the dynamical drive for this model stratosphere is somewhat deficient. The validity of this argument is already suggested in the present model in the sense that the northern hemisphere isoline slopes are noticeably larger than the equivalent southern hemisphere slopes (see Figure 1). This is compatible with the observation that the northern hemisphere of this model is considerably more dynamically active than its southern hemisphere [see *Manabe and Mahlman*, 1976].

These arguments strongly indicate that improvement of this discrepancy is directly dependent upon a solution of the "cold-bias" deficiency of these models. Experience with N₂O modeling in more recent versions of the GFDL "SKYHI" GCM [e.g., *Mahlman and Umscheid*, 1984] has already shown these arguments to be essentially correct; as the cold bias is reduced, the meridional N₂O slopes become steeper.

6. VARIABILITY OF STRATOSPHERIC N₂O

6.1. Longitudinal Variability

In previous N₂O modeling studies we have investigated the spatial and temporal variations of N₂O in the troposphere [Levy and Mahlman, 1980; Levy et al., 1982]. Here we examine the nature of stratospheric N₂O variations and their meteorological and statistical interpretation. Such an analysis can prove to be of much theoretical and practical value.

As in the work by *Levy et al.* [1979], we define the longitudinal (percent) standard deviation as

$$V_{\lambda} = \frac{100}{\langle R \rangle^{\lambda}} [\langle (R - \langle R \rangle^{\lambda})^2 \rangle^{\lambda}]^{1/2} \quad (1)$$

where $\langle \rangle^{\lambda}$ is the zonal mean.

Figure 5 shows meridional cross sections of V_{λ} for the months of January, April, July, and October for the Fast-Sink and January and July for the Slow-Sink N₂O experiments. In this figure, V_{λ} shows very similar structure to that given by

Levy et al. [1979]. In particular, as *Levy et al.* pointed out, the largest values of V_{λ} appear in those regions where the vertical gradient of $\langle R \rangle^{\lambda}$ is the largest. Thus values of the order of 10% appear in the stratosphere, while tropospheric values are less than 1% (much less in the tropics). This wide range in variability for a particular global lifetime demonstrates a serious limitation of the *Junge* [1974] rule relating variability to global lifetime. The association of variability and mean vertical gradient has been made in a more specific and usable way by *Ehhalt et al.* [1983] for temporal variability. This will be addressed in detail later.

Comparison of the N₂O results in Figure 5 shows that the Fast-Sink V_{λ} s are about twice as large as those of the Slow-Sink V_{λ} s (actual range ~ 1.5 – 2.7). These results suggest a simple modification of the *Junge* [1974] rule. A particular form of variability (V_{λ} here) and the global lifetimes for two trace gases a and b have the following approximate relationship for local variability:

$$\frac{V_{\lambda}(a)}{V_{\lambda}(b)} \approx C \frac{\tau(b)}{\tau(a)} \quad (2)$$

where τ represents global lifetime (global amount/global chemical destruction) and C is a constant of order 1. Empirically, here the best fit that encompasses the model data is $C \approx 1.15 \pm 0.35$ (As $\tau(a) \rightarrow \tau(b)$, we expect $C \rightarrow 1$). Thus (2) can be thought of as a modified *Junge* rule but one which retains its extremely simplified character. The limitations of such a simple-type rule will be investigated in the next section.

6.2. Temporal Variability

We now turn toward the problem of understanding the temporal variations of long-lived trace gases. Perhaps the simplest statistical quantity is the temporal (percent) standard deviation V_t , where

$$V_t = \frac{100}{\langle R \rangle^t} [\langle (R - \langle R \rangle^t)^2 \rangle^t]^{1/2} \quad (3)$$

and $\langle \rangle^t$ is the time average over an arbitrary interval.

Shown in Figure 6 are annual N₂O V_t from BAM86 for "Canal Zone" (actually an average of Brazil and Canal Zone), Laramie, and Antarctica compared to the same quantity from model grid points corresponding to these locations for the Fast-Sink and Slow-Sink N₂O experiments. Generally, Figure 6 shows that the "observed" V_t s are greater than the Slow-Sink and Fast-Sink model values. Exceptions to this occur in the lower stratosphere at Canal Zone and Antarctica.

At this time we can only speculate on the cause of these discrepancies. The BAM86 tropospheric V_t s appear to be too large relative to other studies. Whether this is a precision error problem or an analysis inconsistency remains to be determined. The smaller V_t s relative to BAM86 observed near 10 mbar are probably related to the model's too slow decay of N₂O with altitude, especially in mid-latitudes (for further analysis, see section 6.3). It is also possible that vertical velocity fluctuations in the model are suppressed at 10 mbar by the "lid" boundary condition. In addition, measurement errors could be adding significant contamination near 10 mbar. Finally, the better agreement in V_t near 50 mbar at Antarctica is likely to be fortuitous as a result of insufficient sampling at this site. Both $\langle R \rangle^t$ and V_t exhibit fluctuations in the vertical at Antarctica that seem to be related to insufficient sampling (BAM86).

In order that future observational analysis efforts may have some rough guidance on the type of variability to be expected at a given station location, we next present stratospheric time

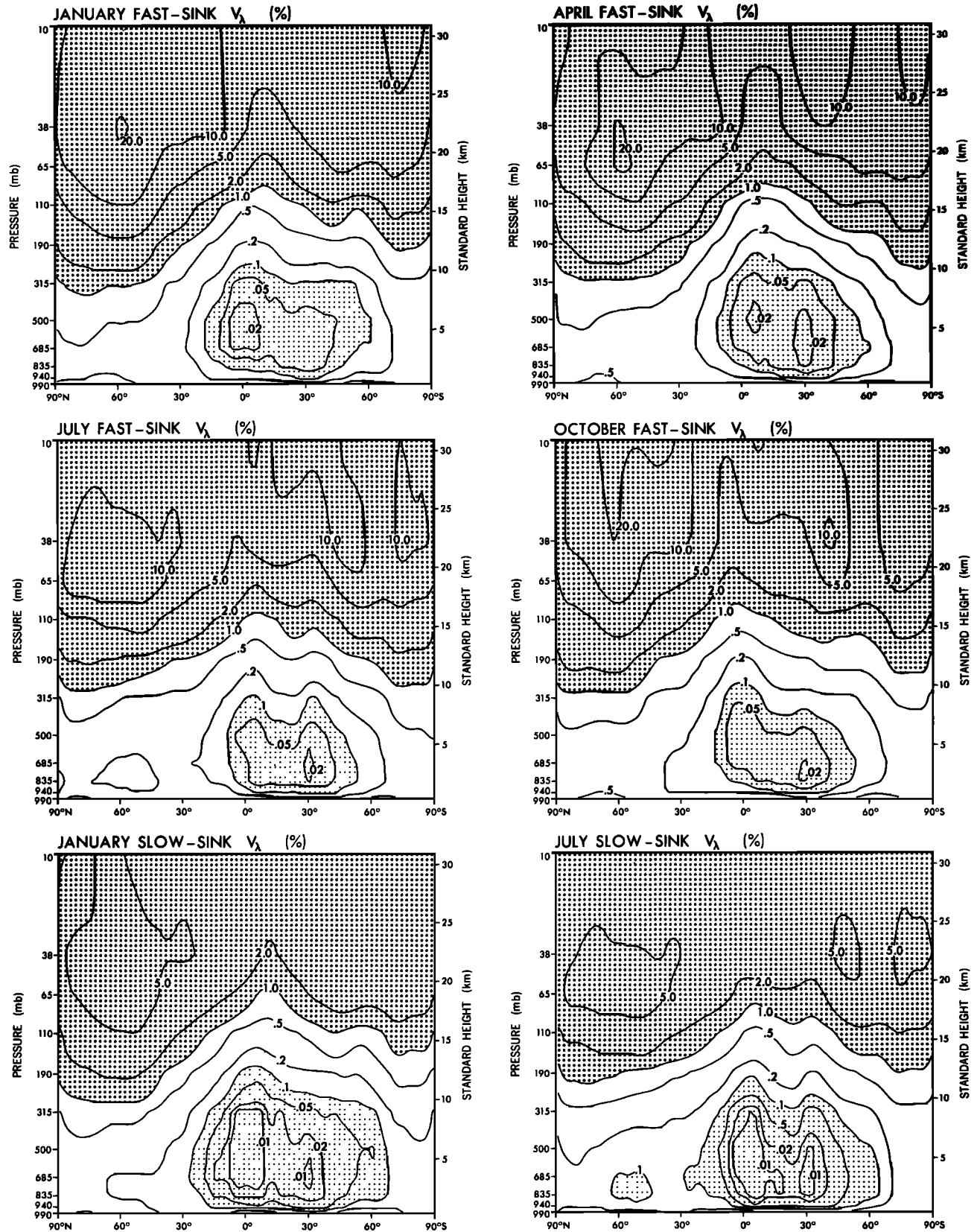


Fig. 5. Longitudinal (percent) standard deviations (V_λ) of N₂O for January, April, July, and October for the Fast-Sink experiment and January and July for the Slow-Sink model experiment.

series from the Regular-Sink N₂O experiment at the same three station locations. Figure 7 shows a 1-year "Canal Zone" (9°N, 80°W) time series at $\sigma = 0.01, 0.038, 0.065,$ and 0.110 from the Regular-Sink N₂O model experiment. Here $\sigma = p/p^*$, where p is pressure and p^* is surface pressure. All levels are plotted on the same scale to show the coherence (or lack of it) between levels. The model "Canal Zone" time series generally shows a weak seasonal cycle, with the exception of a stronger cycle at the $\sigma = 0.038$ level. At that level a midsummer maximum appears, apparently due to a transient local upward R_{N_2O} flux induced by excess diabatic heating under the nearly overhead sun. The weak double maximum (April and October) at $\sigma = 0.01$ (≈ 10 mbar) is in qualitative agreement with the satellite observations at 10 mbar [Jones and Pyle, 1984] (but not to be confused with their spatial double maximum in the upper tropical stratosphere). Note that in the lower stratosphere levels the time series occasionally cross each other. These events are transport-induced local inversions caused mainly by differential horizontal tracer advection. They are relatively rare events in this model but should become more common in higher-resolution models and observed data sets as the vertical resolution is increased. Such inversion events are relatively common in the lower stratosphere for ozone [e.g., Breiland, 1967, 1968; Dobson, 1973].

Shown in Figure 8 are the same type of time series but for the model "Antarctica" (80°S, 128°W) grid point. Here the $\sigma = 0.190$ level has been added. At $\sigma = 0.01$ there is a well-defined seasonal cycle; in fact, the fluctuations on a sub-monthly scale contribute to less than one third of the total variance there. At the other levels the annual cycle is much weaker. At these levels the submonthly fluctuations produce from 70–90% of the total variance, leading to the V_t values shown in Figure 6.

The same type of comparison is shown in Figure 9 for the "Laramie" (41°N, 105°W) grid point. At $\sigma = 0.190$ and 0.110 the annual cycle is rather weak, while at $\sigma = 0.065$ and 0.038 it is more noticeable, with a spring minimum and a fall maximum. This is compatible with the reversed behavior (spring maximum) for "downward moving" substances such as ozone. Note in the lower stratosphere that the number of isoline "crossings" are more numerous than at "Canal Zone" and "Antarctica." This is related to the generally more active northern hemisphere stratospheric dynamics in this model at these levels.

At $\sigma = 0.01$, Figure 9 shows a pronounced annual cycle with a broad spring maximum and a narrower fall minimum. Both the balloon data in BAM86 and satellite data [Jones and Pyle, 1984] show just the opposite phase, similar to both observations and model in the lower stratosphere. This discrepancy provides insight into another model defect.

The late winter-spring minimum in the lower stratosphere is related to the increased poleward-downward movement of air parcels in late winter in association with the intensified wave forcing (and increased polar diabatic cooling). At 10 mbar this wintertime effect is suppressed in the model, probably because of the use of a "lid" boundary condition just above this highest model level. The erroneous winter maximum is produced by an intensified poleward eddy flux in the winter season, as inferred from zonal mean N₂O balances of the kind presented by Mahlman et al. [1980]. Such balances also show the model summer minimum is caused mainly by photodestruction that is apparently not compensated by enough upward N₂O transport during the summertime easterly wind regime. Thus we conclude that the discrepancy results from a suppression of the diabatic vertical velocity at 10 mbar, due mainly to use of

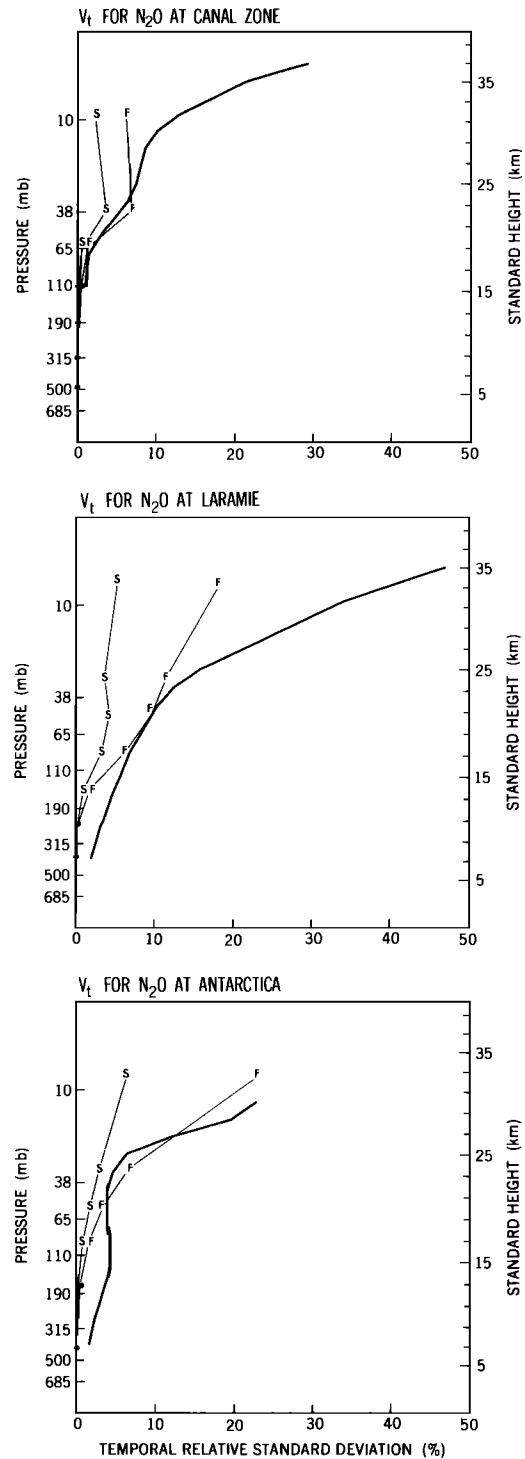


Fig. 6. Profile of temporal (percent) standard deviation (V_t) of N₂O at "Canal Zone" (actually, average of Brazil and Canal Zone stations), Laramie, and Antarctica (heavy line). Also shown are V_t from the Fast-Sink (F) and Slow-Sink (S) N₂O experiments.

the "lid" upper boundary condition, and that the problem is not caused by overactive eddy structures.

A particularly interesting feature of the $\sigma = 0.01$ time series in Figure 9 is the two-stage, mid-September "burst" of large N₂O values. A more careful look shows this sudden increase is not a zonal mean phenomenon but is local to the region in the vicinity of the "Laramie" grid point. This may be seen in Figure 10, which shows regional 10-mbar synoptic charts of

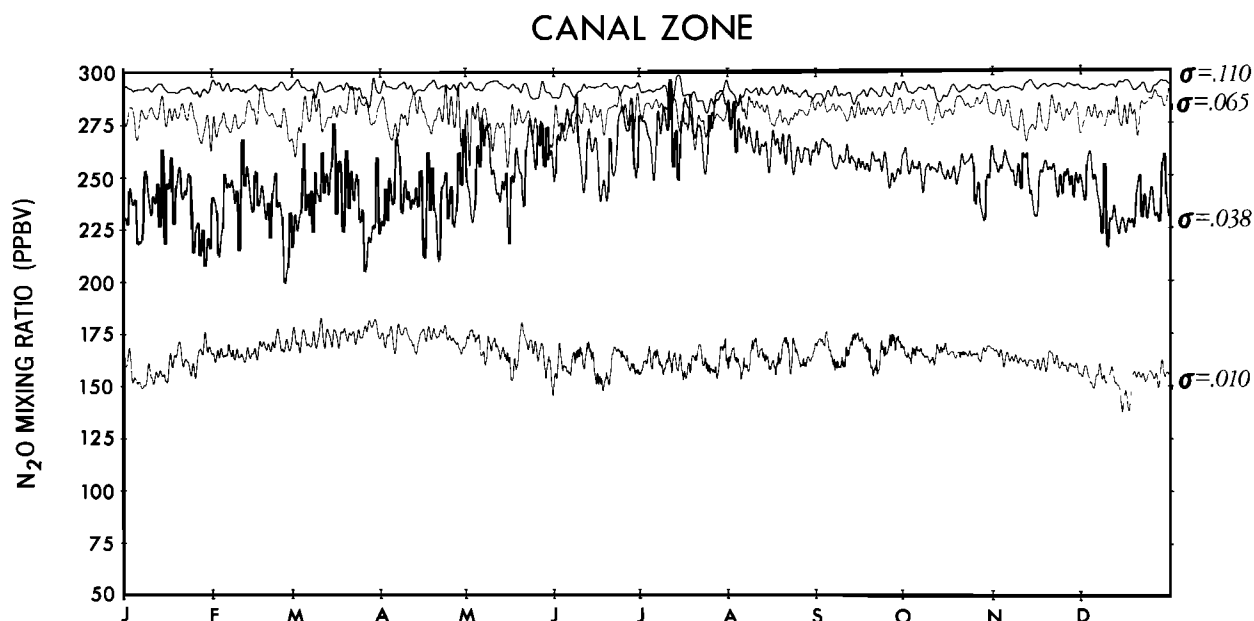


Fig. 7. One-year model N₂O time series from the Regular-Sink N₂O experiment for "Canal Zone" (actually, average of Brazil and Canal Zone stations) at model σ levels 0.01, 0.038, 0.065, and 0.110. Here $\sigma = p/p^*$ where p is pressure and p^* is surface pressure.

R_{N_2O} and model streamlines for the model dates of September 6, 10, 14, and 18. During this period the weak summertime circulation is giving way to the stronger, planetary wave-dominated winter westerlies. Accompanying this transition, an anticyclone forms over the eastern United States. Associated with this formation, a region of tropical N₂O values is drawn poleward over the western United States. Figure 10 for September 10 shows larger N₂O values moving into the western United States as a result of this transient disturbance. These larger N₂O values are sustained over the western half of the United States until an even larger N₂O burst appears on September 18, associated with more southerly flow as the anticyclone over the eastern United States reintensifies. This burst of N₂O is transported irreversibly into mid-latitudes and is associated with transient growth of the subtropical anti-

cyclones separating tropical easterlies from mid-latitude westerlies.

Presently, the observed local N₂O data are not good enough to verify or disallow the occurrence of such phenomena in the actual atmosphere. However, the nature of this model phenomenon is such that there is no reason not to expect such transport events to occur in the real atmosphere as well. Depending on its spatial scale, a specific event may or may not be visible from satellite data. The event described here would be just below the sampling resolution of a typical polar-orbiting satellite ($\sim 30^\circ$ longitude).

6.3. " Δ " Diagnostics

Recently, *Ehhalt et al.* [1983] expanded upon the observation that tracer variability tends to be largest in regions of

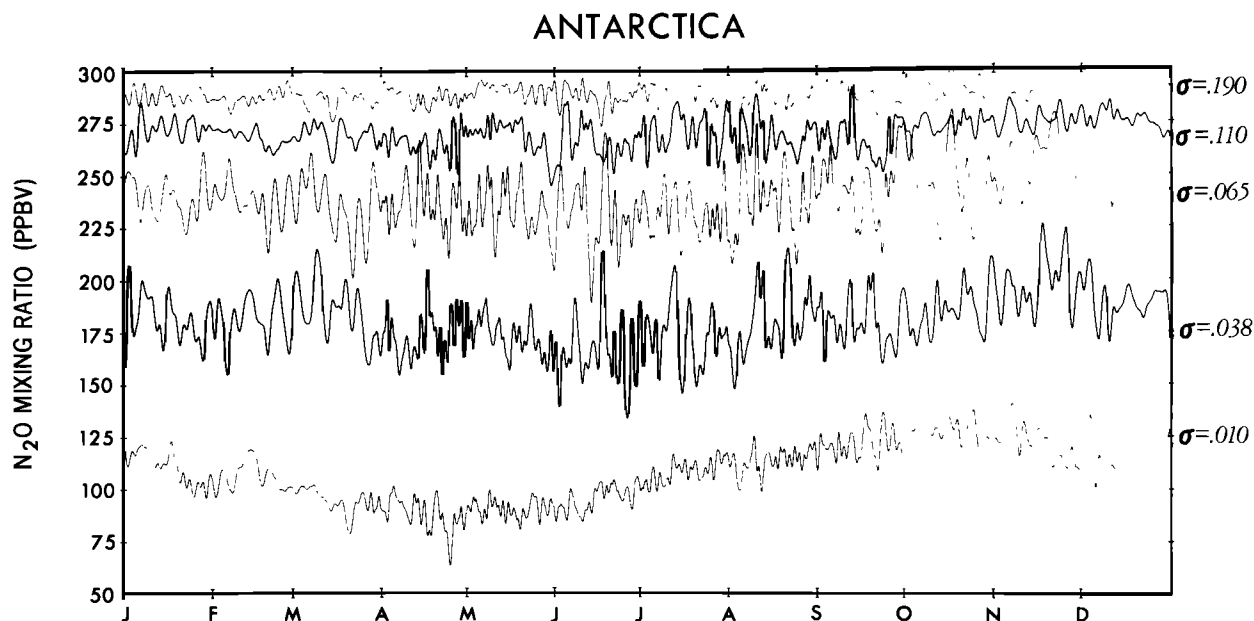


Fig. 8. Same as Figure 7, except at the model grid box corresponding to Antarctica (80°S, 120°W).

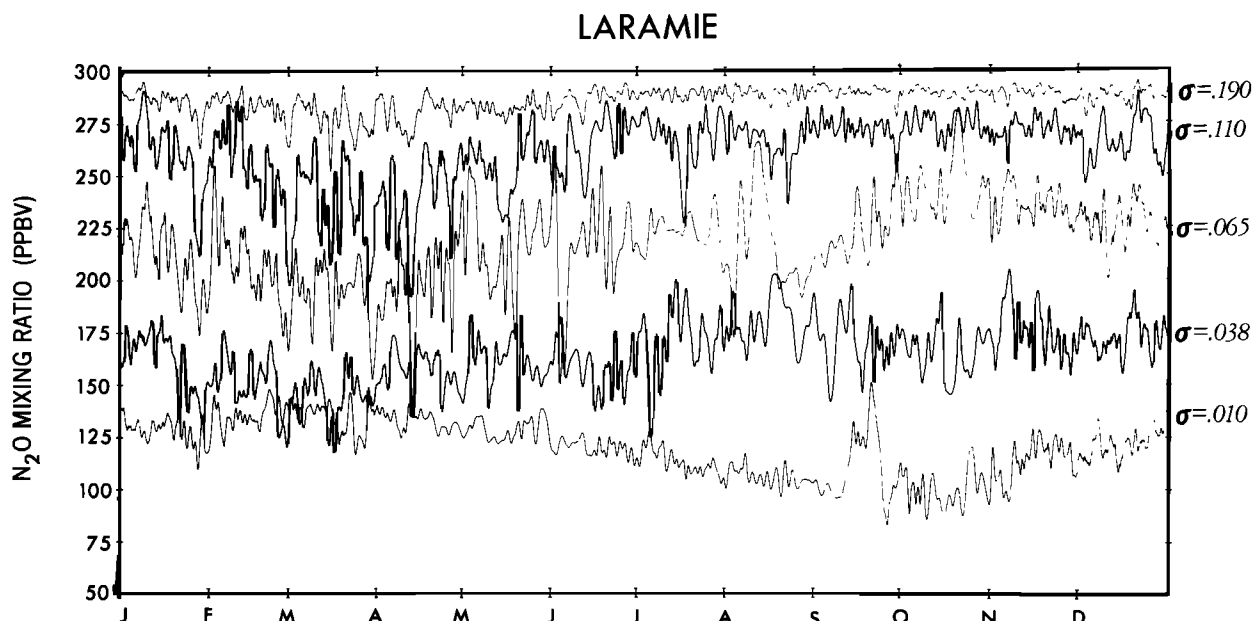


Fig. 9. Same as Figure 7, except at the model grid box corresponding to Laramie, Wyoming (41°N, 105°W).

largest vertical tracer gradient [e.g., *Levy et al.*, 1979]. They defined a new quantity, the “equivalent displacement height,”

$$\Delta \equiv \frac{[\langle (R - \langle R \rangle)^2 \rangle]^{1/2}}{(\partial \langle R \rangle / \partial z)} \quad (4)$$

Thus Δ is simply the temporal standard deviation divided by the time mean vertical gradient. Alternatively, it can be defined as $V_i / \partial \ln \langle \bar{R} \rangle / \partial z$.

Shown in Figure 11 are N₂O Δ values calculated for Laramie, Wyoming, from BAM86 and from the three N₂O experiments described here. These Δ values have been compared against Δ s for the same conditions from the “Slow-Destruction” three-dimensional ozone model experiment of *Levy et al.* [1985]. The results are very similar to those of Figure 11; an exception appears at 10 mbar, where the ozone chemistry is very fast. Thus the model shows an even stronger agreement of Δ s than that given in the more limited data sets used by *Ehhalt et al.* [1983]. We conclude that their original assertion on the usefulness of Δ is indeed correct. Furthermore, Figure 11 shows that the model Δ values agree reasonably well with the Δ s from the BAM86 analysis. In each case, Δ has a minimum of about 1 km in the lower stratosphere, rising to several kilometers in the upper troposphere and in the middle stratosphere. The striking agreement of the model Δ s with the observational results of BAM86 suggests strongly that the model V_i deficiency shown in Figure 6 arises mainly from the model’s excessively weak vertical gradients at Laramie (too weak meridional slopes).

Note also that the Δ values in Figure 11 are not identical, even for the “perfect” model data. The three N₂O experiments are very similar, but the midstratospheric Δ s for the Fast-Sink N₂O are generally smaller than for Regular-Sink and Slow-Sink N₂O. The largest Δ values are found in Slow-Sink N₂O. These small but systematic differences in Δ for different trace constituents lead us to seek an explanation for such differences.

7. THEORETICAL INTERPRETATION OF “ Δ ” STATISTICS

The numerical results of section 6 show small but noticeable differences in Δ magnitudes for different modeled N₂O de-

struction scenarios. Because of the availability of detailed results from the three-dimensional model as well as insights from the previous analyses in this paper, we offer a different perspective on the significance of Δ than that given by *Ehhalt et al.* [1983]. In particular, we emphasize the factors leading to differences in Δ for different trace constituents.

First, we write the general trace constituent continuity equation in log pressure coordinates as

$$\frac{\partial R}{\partial t} = -\mathbf{V}_3 \cdot \nabla_3 R + \nabla_2 \cdot \mathbf{K}_H \nabla_2 R + \frac{1}{\rho_s} \frac{\partial}{\partial z} \rho_s K_v \frac{\partial R}{\partial z} + \text{SMS} \quad (5)$$

where the log pressure coordinate and associated variables z and ρ_s are defined as in the appendix, K_H and K_v are horizontal and vertical subgrid-scale diffusion coefficients used in the three-dimensional model, \mathbf{V}_3 and ∇_3 the three-dimensional vector velocity and gradient operator in log pressure coordinates, ∇_2 the horizontal gradient operator and SMS is the net of all chemical/physical sources minus sinks.

Multiplying (5) by $R' = R - \langle R \rangle'$ and time averaging, we obtain the trace constituent eddy variance equation

$$\frac{\partial \langle R'^2 \rangle}{\partial t} = -\langle \mathbf{V}_3' R' \cdot \nabla_3 \langle \bar{R} \rangle' \rangle - \left\langle \mathbf{V}_3 \cdot \nabla_3 \frac{R'^2}{2} \right\rangle + \langle R' \nabla_2 \cdot \mathbf{K}_H \nabla R' \rangle + \left\langle \frac{R'}{\rho_s} \frac{\partial}{\partial z} \rho_s K_v \frac{\partial R'}{\partial z} \right\rangle + \langle R' \text{SMS}' \rangle \quad (6)$$

In (6) the right-hand side terms from left to right are the temporal variance production, the variance advection by mean and transient motions, the horizontal variance dissipation, the vertical variance dissipation, and the variance production or dissipation by chemical changes (usually dissipation), respectively.

It is worth noting that the conceptual model developed below is fundamentally different from the usual mechanistic approaches [e.g., *Plumb*, 1979]. In that type of development the transient tracer R' is viewed as evolving in time from a small amplitude perturbation on a time mean background state. In this work we visualize the transient tracer field as

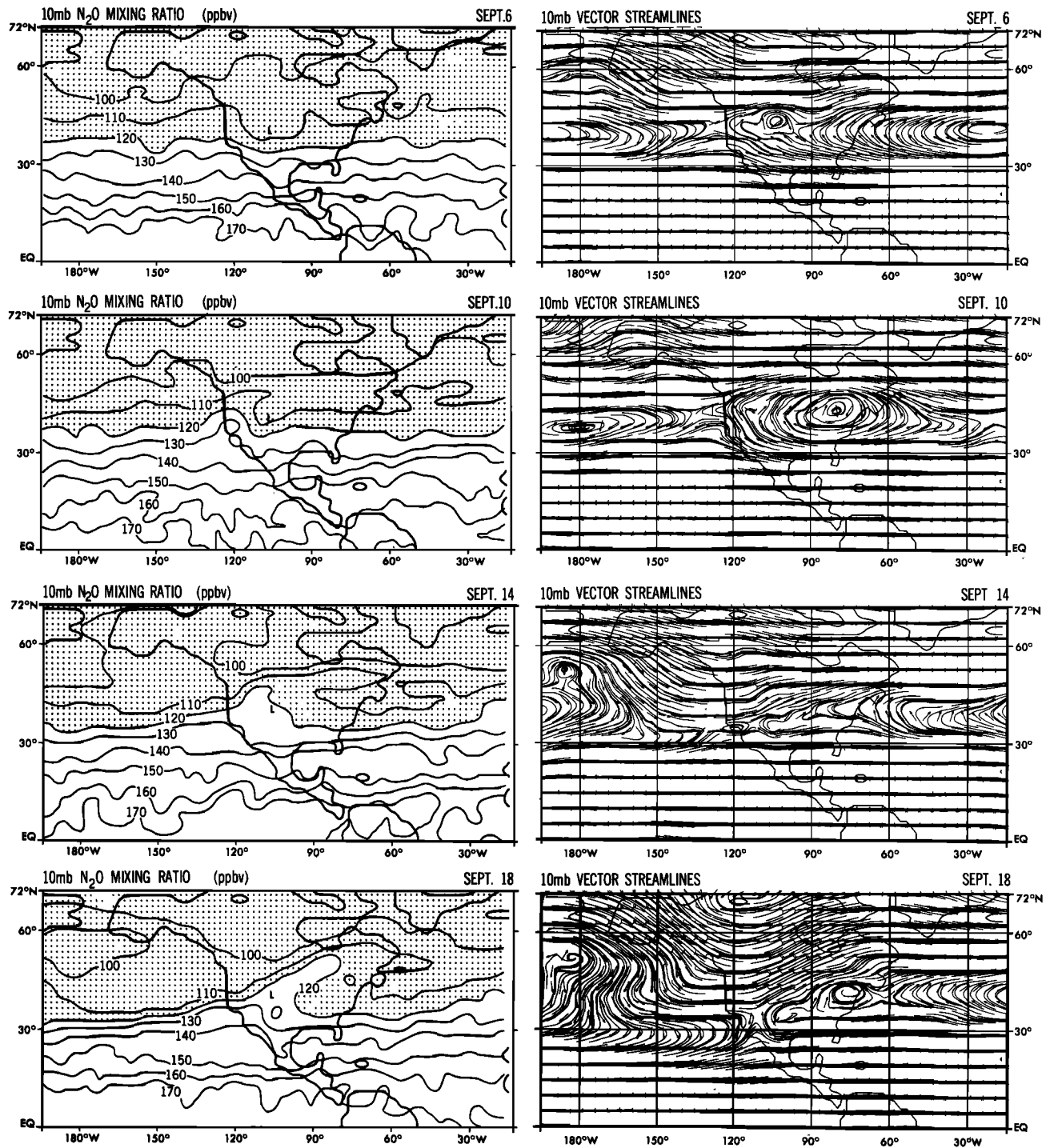


Fig. 10. Instantaneous 10-mbar charts of N₂O mixing ratio (left, ppbv) and wind vector/streamlines (right). Each wind barb equals 10 m s⁻¹. Dates shown are for September 6, 10, 14, and 18. Small "L" marks Laramie location.

being ever present at nonnegligible amplitude. Accordingly, the approximate long-term balance is between production/advection of transient variance and its dissipation. For time-averaged statistics the temporal evolution term in (6) is negligible.

Now we proceed by introducing the following definitions:

$$C_m \equiv - \frac{\langle R' \nabla_2 \cdot K_H \nabla_2 R' \rangle^t + \langle (R' / \rho_a) \partial / \partial z \rho_s K_v (\partial R' / \partial z) \rangle^t}{\langle R'^2 \rangle^t} \quad (7)$$

$$C_c \equiv - \frac{\langle R' S M S' \rangle^t}{\langle R'^2 \rangle^t} \quad (8)$$

Here C_m^{-1} can be thought of as a mechanical dissipation time and C_c^{-1} as a chemical-damping time. These quantities, C_m and C_c , can be visualized as being computed in advance by the three-dimensional model for a given trace constituent. A priori, there is no proof that C_m , let along C_c , should be the same for different trace constituents. Nevertheless, we make conceptual progress by condensing these intrinsically difficult terms, substituting (7) and (8) into (6) to obtain

$$\frac{\partial \langle R'^2 \rangle^t}{\partial t} = - \langle \mathbf{V}_3 R' \rangle^t \cdot \nabla_3 \langle R' \rangle^t - \left\langle \mathbf{V}_3 \cdot \nabla_3 \frac{R'^2}{2} \right\rangle^t - (C_m + C_c) \langle R'^2 \rangle^t \quad (9)$$

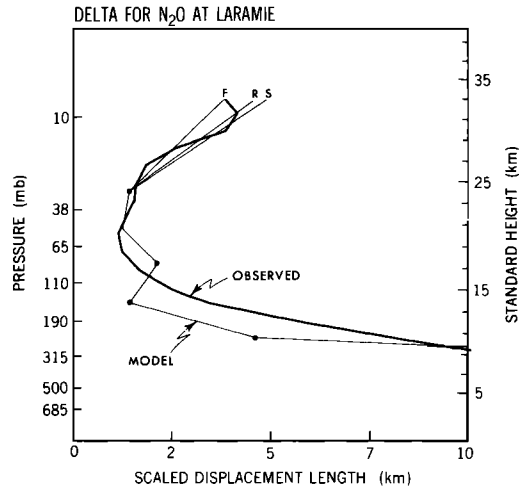


Fig. 11. Annual mean N₂O “Δ” profile (scaled displacement length) at Laramie, Wyoming (41°N, 105°W) from the BAM86 analysis (For definition, see (4)). Also shown are model N₂O Δ profiles for the “Laramie” location from the Fast-Sink (F), Regular-Sink (R), and Slow-Sink (S) N₂O experiments.

At statistical equilibrium (or with sufficiently long time averaging), (9) becomes

$$\langle R'^2 \rangle' = \frac{-\langle \mathbf{V}_3' R' \rangle' \cdot \nabla_3 \langle R \rangle' - \langle \mathbf{V}_3 \cdot \nabla_3 (R'^2/2) \rangle'}{C_m + C_c} \quad (10)$$

The first term in the numerator of (10) is the familiar production of temporal variance by a net transient flux of R down the time mean gradient of R . The second term represents the average advection of transient variance into a given region by mean and transient winds. Roughly speaking, if upstream of a chosen point is a region of large production of $\langle R'^2 \rangle'$, the tendency of this R'^2 to be “blown downstream” would act to increase the local transient variance. Conversely, if the upstream area is a quiet one in terms of transient variance production, then this advection would act to decrease the local variance. Thus this term can readily be either positive or negative, depending on location. Here we will simplify the treatment of this term by considering only the advection of temporal variance by the time mean state (or equivalently, that the triple product term in equation (10) is negligible). Also, we will assume for convenience that the spatial gradients of $\partial \langle R \rangle' / \partial z$ are small relative to spatial gradients of $\langle R'^2 \rangle'$. These assumptions lead to essentially the same result as using linear theory directly to derive (10).

Now working on the first term in (10), we note that the only transient eddy flux of R of interest here is the statistically averaged component normal to the gradient of $\langle R \rangle'$. Accordingly, we describe this statistical quantity (generated explicitly by the three-dimensional model) as an effective symmetric diffusion process. We thus assume that locally

$$\begin{aligned} \langle u' R' \rangle' &= -K_x^* \frac{\partial \langle R \rangle'}{\partial x} & \langle v' R' \rangle' &= -K_y^* \frac{\partial \langle R \rangle'}{\partial y} \\ \langle w' R' \rangle' &= -K_z^* \frac{\partial \langle R \rangle'}{\partial z} \end{aligned} \quad (11)$$

Note that these K^* s are not the same as the subgrid-scale coefficients used in the three-dimensional model, nor are they at all similar to the effective K s defined in the appendix. Here these K^* s represent the net statistical effect of transient motions to transfer R down its time mean gradients. The actual physics of this process is an extremely complicated mix of advective processes setting up diffusive processes and can only

rationally be attacked in a reasonably high-resolution three-dimensional GCM (if then!). Note, in principle, that these K^* s can vary for different trace constituents.

We now substitute the definitions (11) into (10), divide by $(\partial \langle R \rangle' / \partial z)^2$ and use the simplifications indicated above to obtain

$$\begin{aligned} \Delta^2 \equiv \frac{\langle R'^2 \rangle'}{[(\partial \langle R \rangle' / \partial z)^2]} &\approx K_x^* [(\partial z / \partial x_{\langle R \rangle'})^2] + K_y^* [(\partial z / \partial y_{\langle R \rangle'})^2] \\ &+ K_z^* - \frac{1}{2} \langle \mathbf{V}_3 \rangle' \cdot \nabla_3 (\Delta^2) + \dots (C_m + C_c)^{-1} \end{aligned} \quad (12)$$

In (12) we have used the definitions

$$\frac{\partial z}{\partial y_{\langle R \rangle'}} = -\frac{(\partial \langle R \rangle' / \partial y)}{(\partial \langle R \rangle' / \partial z)} \quad \frac{\partial z}{\partial x_{\langle R \rangle'}} = -\frac{(\partial \langle R \rangle' / \partial x)}{(\partial \langle R \rangle' / \partial z)} \quad (13)$$

which, similar to the appendix, define the time mean slopes of equilibrium trace constituent mixing ratio surfaces.

The quality Δ in (12) is the same as that defined by *Ehhalt et al.* [1983]. Thus we are now in a position to investigate more carefully why Δ , the “equivalent displacement height,” exhibits such useful properties. Furthermore, it allows us to carry into the time domain our effort in this paper to predict future trace constituent behavior on the basis of a small number of GCM integrations to statistical equilibrium.

Inspection of (12) tells us that if trace constituents a and b are: (1) almost chemically conservative ($C_c \ll C_m$), (2) have the same effective K^* s, (3) have the same $\langle R \rangle'$ “topography,” and (4) omitted higher-order terms are negligible, then

$$\Delta_a^2 = \Delta_b^2$$

provided we further note that if the Δ s are equal, then the advection of Δ s in (12) would also be equal.

The above arguments provide an explanation for why Δ is essentially the same in the lower stratosphere for the three model experiments, as shown in Figure 11. In that altitude range, $C_c \rightarrow 0$ and the “topography” of the $\langle R \rangle'$ surfaces is essentially identical, as pointed out in section 3. Further, we expect the K^* s to be more or less the same for different trace constituents as long as the chemistry is sufficiently slow (and perhaps the mechanical dissipation of R variations has the same character for each trace gas).

Inspection of (12) also justifies the caution of *Ehhalt et al.* [1983] in interpreting Δ literally as a vertical displacement, as might be superficially inferred from the vertical gradient dependence. As shown in the appendix, the equilibrium tracer slopes represent a tight coupling between horizontal and vertical transport/chemical processes. Evaluation of (12) and the basic components of $\langle -\mathbf{V}_3' R' \rangle' \cdot \nabla_3 \langle R \rangle'$ from the GCM suggests a crude isotropy in the production of Δ^2 ; the east-west and north-south tracer slopes approximately compensate for the large differences in effective K^* s ($K_x^* > K_y^* \gg K_z^*$). Another way to illustrate this is to redefine a Δ leading to (12) by dividing by the meridional gradient $(\partial \langle R \rangle' / \partial y)$. In this case the modified Δ s so produced have magnitudes of ~ 1000 km. Therefore we conclude that Δ should be thought of as a “scaled displacement length,” because the definition of Δ carries no implications of dominance of displacement from one coordinate direction over another. However, “equivalent displacement height” remains an appropriate description for Δ as long as it is recognized that transient R perturbations can come from any coordinate direction with more or less equal probability for a tracer in statistical equilibrium.

Next we explore circumstances under which Δ_a is predicted to be different than Δ_b . First, in (12) if $C_c \geq C_m$, it would have a direct damping effect on the calculated Δ as a result of this accelerated temporal variance destruction. Superficially, this is

a rather weak constraint, since $C_m^{-1} \sim 10\text{--}20$ days (at least in this GCM for the lower stratosphere). Thus two trace constituents, one with $C_c^{-1} \sim 50$ days and one with $C_c^{-1} = 500$ days, would appear to be predicted to exhibit very nearly the same Δ value. However, this apparently is not the case. Even slower chemical destructions enter the problem indirectly through their influence on the equilibrium R slope appearing in the numerator of (12). The theoretical model of the appendix (as illustrated in Figure A1) shows that significant tracer slope flattening is expected for chemical destruction times ranging from $\sim 10\text{--}1000$ days.

Thus the combined analyses of the appendix and (12) predict an observable decrease in Δ for a "shorter" long-lived trace constituent such as CFCl_3 , relative to other gases such as N_2O or CF_2Cl_2 . The physical interpretation of this predicted Δ reduction for gases such as CFCl_3 is straightforward in the sense that as the equilibrium $\langle R \rangle'$ surfaces become flatter, the opportunity for horizontal displacements to contribute to Δ become reduced.

Finally, as the chemical destruction becomes fast relative to C_m , it is likely that the K^* s and the gradients of Δ^2 in (12) would also change. At this fast destruction limit it is not presently possible to predict the influence these additional processes would have on the determination of Δ .

The predictive capability implied in (12) has been tested in the three-dimensional model for the Fast-Sink and Slow-Sink experiments, using the $\approx 20\%$ Fast-Sink reduction in slope between 38 and 10 mbar, as noted at the end of section 3.2. This calculation predicts that Fast-Sink N_2O at Laramie over this layer should have a Δ of about 15% lower (for a factor of 3 increase in photodestruction rate) than that for Slow-Sink N_2O . The actual difference in the three-dimensional model is about 20%. Given the crudeness of the calculations, this agreement is rather close.

The above prediction of a reduced Δ for long-lived gases with faster-destruction times was also tested in the observational study of BAM86. Unfortunately, their results were inconclusive. If anything, the Δ values for (faster destruction) CFCl_3 might be greater than for CF_2Cl_2 and N_2O . However, they point out that the sampling error for calculation of Δ is so large (especially for CFCl_3) that no statistically significant identification of Δ differences can be made from their data set. Thus the prediction of small, but illuminating, differences in Δ statistics must await more complete data sets with higher-precision measurements.

Finally, we note the possibility of circumstances in which the simple equilibrium Δ^2 model of (12) may be inappropriate. For short sampling intervals or circumstances following seasonal transitions the assumptions leading to (12) may not hold.

An important example of such a possibility is given by Hess and Holton [1985]. They address the relatively large Δ^2 values measured by Ehhalt *et al.* [1983] for summer mid-latitudes. Using a mechanistic model, they hypothesize that the relatively large Δ^2 values are "frozen" in the zonal flow following the large meridional exchange near the descending zero zonal wind line associated with the transition to summertime easterlies (e.g., see Dickinson [1969]; Mahlman and Moxim [1978]). These large tracer perturbations thus get caught in the easterly flow and are simply advected zonally.

Such a localized circumstance suggests a more complex interpretation of the framework given in (6)–(12). During the zonal wind reversal, Δ^2 values would be increased substantially as a result of enhancements of the variance production terms. In the summertime easterlies, both production and dis-

sipation C_m are rather weak; the high Δ^2 values are simply advected past a point by the zonal easterly flow. For such a short period the direct balance between production and dissipation controlling the Δ^2 amounts in (12) is not realized. However, for annual statistics the balance in (12) should be a good approximation.

8. SUMMARY AND CONCLUSIONS

In this paper we have described three stratospheric N_2O experiments using the GFDL general circulation/tracer model. The first experiment (Regular-Sink N_2O) uses stratospheric photodestruction coefficients thought to be correct in the mid-1970's. The second experiment (Slow-Sink N_2O) uses the temperature-dependent absorption cross sections introduced by Selwyn *et al.* [1977] as well as other chemical data current in 1980. However, this choice produces too much N_2O in the middle stratosphere. To investigate the possibility of the modeled stratospheric N_2O losses being too weak, a third experiment (Fast-Sink N_2O) was run which uses doubled values of the photodestruction coefficients from the Regular-Sink N_2O experiment.

The three N_2O three-dimensional model experiments have been compared in detail against the detailed observational analysis of J. T. Bacmeister *et al.* (unpublished manuscript, 1986) (BAM86). In terms of one-dimensional structure, the observations are most like a model somewhat midway between the Regular-Sink and Fast-Sink N_2O experiments. This suggests the possibility of required faster N_2O removal, as indicated by the inferences of lower O_2 absorption cross sections by Frederick and Mentall [1982].

Integration and analysis of these three N_2O experiments revealed some interesting behavior. It was found that the Fast-Sink and Slow-Sink N_2O experiments exhibit predictable globally averaged (one-dimensional) behavior, given the results from the Regular-Sink N_2O experiment. Specifically, the set of global one-dimensional eddy diffusion coefficients (K_z s) producing consistent globally averaged behavior for one experiment were found to produce excellent predictions of the one-dimensional behavior of the other two experiments. Furthermore, it was found that the meridional slopes of N_2O isolines are virtually identical in the lower stratosphere for the three N_2O experiments.

The generality of the above two results was investigated through use of a simple theoretical two-slab model. In this model the transport balances leading to equilibrium meridional mixing ratio slopes are solved explicitly. Specifically, the simple model shows that meridional mixing ratio slopes are the same for a wide class of trace constituents, given a very slow destruction (or production) chemistry. For gases with moderate to fast photodestruction rates, the effect is to flatten the meridional slopes.

In addition, the two-slab model shows a physical basis for the one-dimensional global eddy diffusion coefficient K_z . In this model, K_z depends upon the meridional slope of a given constituent (which in turn depends upon the chemical destruction rate). Also, K_z depends upon the intensity in which upward propagating disturbances from the troposphere force the stratospheric zonal winds. Finally, the two-slab model shows that the meridional isoline slope in turn depends upon the K_z value, although in most cases the dependence is comparatively weak. The two-slab model thus predicts that the apparent "universality" of meridional slopes and K_z for N_2O fortuitously arise from the relative weakness of the prescribed destruction chemistries. Tracers with stronger chemistries are predicted to exhibit noticeably different behavior. Conse-

quently, this simple theoretical model can be used to predict meridional slopes and effective one-dimensional K_z s for a wide class of longer-lived trace gases.

Comparison of the model meridional mixing ratio slopes against the climatologies of BAM86 indicate that the model slopes are too flat by about 30%. By using the predicted slope structure from the simple two-slab model we infer that the basic cause of this deficiency is a too weak dynamical forcing of the zonal winds in the model stratosphere. This leads to a situation in which the polar temperatures are too cold, and the model temperatures are too close to their radiative equilibrium limits. Thus we conclude that this discrepancy has the same roots as that of the well-known polar cold bias of this and other GCM's.

A detailed comparison of the model's temporal variability has been made against the BAM86 N₂O climatology. Generally, model and observation show reasonable agreement except near 10 mbar, where the observed variabilities are significantly larger, and the higher-latitude seasonal cycle is out of phase. The model temporal standard deviations have been divided by the time mean vertical mixing ratio gradient to yield a quantity "Δ." This Δ has been shown by *Ehhalt et al.* [1983] to reveal a remarkable unity among a wide class of constituents. This model essentially verifies the wide range of applicability of using Δ statistics.

A simple theoretical model has been developed which shows why Δ statistics are so often similar for different trace gases. Also, the simple model offers specific predictions of the conditions under which Δs should differ among various trace constituents. These predictions agree with the three-dimensional model behavior but may disagree with the BAM86 observations. Unfortunately, the observed data are not good enough to isolate any meaningful statistical significance. Thus a full test of this prediction awaits further observations and analysis.

Finally, detailed profile time series are presented from the model for those station locations used in the BAM86 observational analyses. These time series, along with supporting model horizontal charts, show a complex behavior with pronounced seasonal cycles, local transport induced "inversions," and detailed meridional transport events associated mainly with seasonal transitions and transient disturbances. Such time series, in addition to the other model results, can allow an evaluation of the sampling required for studies such as BAM86 to resolve fuller details of the local climatologies of various long-lived trace gases.

APPENDIX: A SIMPLE MODEL FOR ASSESSING THE INFLUENCE OF CHEMISTRY ON MERIDIONAL TRACER SLOPES AND VERTICAL TRANSPORT

In section 3 it was shown for this model that suitably long-lived trace gases all exhibit the same equilibrium poleward-downward slopes of mean mixing ratio isolines. The observational study of BAM86 showed this to be true for N₂O and CF₂Cl₂. However, the mean slope for CFCl₃ is flatter than those of the other two, apparently because of the faster photo-destruction chemistry appropriate for CFCl₃.

The purpose of this appendix is to develop a simple model that isolates the essential physical processes leading to equilibrium tracer slopes in the presence of chemical destruction. Here we have in mind the rather large class of atmospheric trace constituents characterized by a tropospheric source and a stratospheric destruction. To accomplish this, we introduce a two-slab model which breaks the meridional plane into two equal-area regions, 0–30° and 30–90° latitude. Here $\langle \rangle^r$

represents a spherical coordinate average over the "tropical" slab and $\langle \rangle^h$ is the average over the "high-latitude" slab. The meridional distance between slabs and across slabs is chosen to be a single, spherical geometry consistent value y . With this we can utilize a Cartesianlike model, while incorporating the important aspects of the spherical geometry. In this model the hemispheric average is given by $\langle \rangle^h = \frac{1}{2}[\langle \rangle^r + \langle \rangle^h]$.

Now consider the simplest possible model that captures the essence of the basic processes controlling the meridional slope of zonal, time mean isolines of tracer mixing ratio. Following the physical model of *Mahlman et al.* [1984], in isentropic coordinates the structure of trace constituent transport in the meridional plane can be thought of crudely as a balance between an advection by the diabatic circulation [*Dunkerton*, 1978] (ultimately forced by dissipating tropospheric disturbances) and a meridional diffusion (caused by the same tropospheric disturbances) (see also *Holton* [1980]). For a more detailed numerical justification, see *Mahlman* [1985]. In this ultrasimplified form, the two-dimensional trace constituent continuity equation can be written as

$$\frac{\partial \langle R \rangle^\lambda}{\partial t} = -W_d \frac{\partial \langle R \rangle^\lambda}{\partial z} - V_d \frac{\partial \langle R \rangle^\lambda}{a \partial \phi} + \frac{1}{a \cos \phi} \frac{\partial}{\partial \phi} K_y \cos \frac{\partial \langle R \rangle^\lambda}{a \partial \phi} - C(y, z) \langle R \rangle^\lambda \quad (\text{A1})$$

where $\langle \rangle^\lambda$ is a zonal average, a is the earth's radius, K_y is an effective meridional diffusion coefficient, and C is a photo-destruction coefficient which, in general, varies with latitude and height. Also, W_d is the diabatic vertical velocity [$W_d = Q/c_p/(g/c_p + \partial T_0/\partial z)$], where Q is the diabatic heating rate, c_p the specific heat at constant pressure, and T_0 is a reference temperature assumed to be a constant 240°K. The quantity V_d is the diabatic meridional velocity compatible with the mass continuity equation

$$\frac{1}{a \cos \phi} \frac{\partial}{\partial \phi} V_d \cos \phi + \frac{1}{\rho_s} \frac{\partial}{\partial z} \rho_s W_d = 0 \quad (\text{A2})$$

expressed in spherical, log pressure coordinates, where $z = H_0 \ln(p_0/p)$. Here, H is the scale height ($H_0 = R^*T_0/mg$), p_0 a standard surface pressure of 1013.25 mbar, R^* the universal gas constant, g the acceleration of gravity, m the molecular weight of dry air, and $\rho_s = mp/R^*T_0$ the standard density. Note that we use log pressure, rather than isentropic coordinates. Given the simplicity of the model chosen here, there is little to gain through explicit use of isentropic coordinates.

Within the two-slab approximation, we average (A2) by integrating over the area from 0°–30° and divide by the 0°–30° area ($A_r = 2\pi a^2 \sin 30^\circ$) to get

$$\frac{V_{30}}{a \tan 30^\circ} = - \frac{1}{\rho_s \sin 30^\circ} \int_0^{30^\circ} \frac{\partial}{\partial z} \rho_s W_d \cos \phi d\phi \quad (\text{A3})$$

where V_{30} is the diabatic meridional velocity at 30°, and $V_0 = V_{90} = 0$ by the lateral boundary conditions. In this problem, $a \times \tan 30^\circ$ becomes the appropriate length scale. Thus we choose

$$y = a \times \tan 30^\circ = 3678.3 \text{ km}$$

With the two-slab model assertion that the only significant vertical velocity in the tropical slab is the average of W_d (W_r), (A3) becomes

$$V_{30} = - \frac{y}{\rho_s} \frac{\partial}{\partial z} \rho_s W_r \quad (\text{A4})$$

The horizontal average of (A2) is

$$\frac{\partial}{\partial z} \rho_s \langle W_d \rangle^H = 0 \quad (\text{A5})$$

Given the boundary condition $\rho_s W_d \rightarrow 0$ as $z \rightarrow \infty$, this implies

$$\langle W_d \rangle^H = \frac{W_{tr} + W_{hl}}{2} = 0 \quad (\text{A6})$$

or

$$W_{tr} = -W_{hl} \quad (\text{A7})$$

We introduce the following two-slab equations and definitions:

$$\langle R \rangle^H = \frac{\langle R \rangle^{tr} + \langle R \rangle^{hl}}{2} \quad (\text{A8})$$

$$\frac{\partial \langle R \rangle^H}{\partial z} = \frac{\partial \langle R \rangle^{tr} / \partial z + \partial \langle R \rangle^{hl} / \partial z}{2} \quad (\text{A9})$$

$$\langle C \rangle^H = \frac{\langle C \rangle^{tr} + \langle C \rangle^{hl}}{2} \quad (\text{A10})$$

$$\frac{\partial z}{\partial y_R} = \frac{-(\partial \langle R \rangle^{\lambda} / \partial y)}{(\partial \langle R \rangle^{\lambda} / \partial z)} \approx \frac{-(\langle R \rangle^{hl} - \langle R \rangle^{tr}) / y}{(\partial \langle R \rangle^H / \partial z)} \quad (\text{A11})$$

Equation (A11) thus defines a simplified meridional tracer slope compatible with the two-slab model approximation. As we shall see, this allows substantial simplifying progress.

To express horizontal terms from (A1) in the two-slab model, some additional manipulations are required. The horizontal diffusion for the tropical slab is given by

$$\begin{aligned} \left\langle \frac{1}{a \cos \phi} \frac{\partial}{\partial \phi} K_y \cos \phi \frac{\partial \langle R \rangle^{\lambda}}{a \partial \phi} \right\rangle^{tr} &= \frac{1}{2\pi a^2 \sin 30^\circ} \\ &\int_0^{30^\circ} \frac{1}{a \cos \phi} \frac{\partial}{\partial \phi} K_y \cos \phi \frac{\partial \langle R \rangle^{\lambda}}{a \partial \phi} a \cos \phi d\lambda a d\phi \\ &= \frac{K_y}{a \tan 30^\circ} \frac{\partial \langle R \rangle^{\lambda}}{a \partial \phi_{30^\circ}} \approx \frac{K_y (\langle R \rangle^{hl} - \langle R \rangle^{tr})}{y^2} \end{aligned} \quad (\text{A12})$$

and with the opposite sign for the high-latitude slab, under the assumption that there is no flux through the equatorial and polar boundaries. Here it is assumed that the meridional length associated with the finite differencing of $\partial \langle R \rangle^{\lambda} / a \partial \phi_{30^\circ}$ is the same as that given previously by $y = a \tan 30^\circ$. The actual choice of length to compute the meridional derivative $\partial \langle R \rangle^{\lambda} / a \partial \phi$ is somewhat ambiguous in the two-slab context. However, the meridional distance between the area-weighted midpoints of the two slabs gives a length that is larger than the earlier choice by only about 3%.

For the horizontal advection term ($V_d \partial \langle R \rangle^{\lambda} / a \partial \phi$) in (A1) we choose a form for the advection that is consistent with a flux form required later for the global mean transport equation. Analytically, this is

$$\begin{aligned} \left\langle -\rho_s V_d \frac{\partial \langle R \rangle^{\lambda}}{\partial y} \right\rangle^{tr} &= - \left\langle \frac{1}{a \cos \phi} \frac{\partial}{\partial \phi} \rho_s \cos \phi \langle V_d \rangle^{\lambda} \langle R \rangle^{\lambda} \right\rangle^{tr} \\ &+ \left\langle \frac{\langle R \rangle^{\lambda}}{a \cos \phi} \frac{\partial}{\partial \phi} \cos \phi \langle V_d \rangle^{\lambda} \right\rangle^{tr} \end{aligned} \quad (\text{A13a})$$

Now using the "box method" rules of *Kurihara and Holloway* [1967] and the spherical coordinate-averaging rules of (A12)

in the two-slab model we get

$$\begin{aligned} \left\langle -V_d \frac{\partial \langle R \rangle^{\lambda}}{a \partial \phi} \right\rangle^{tr} &\approx - \frac{\rho_s V_{30} \langle R \rangle^{hl} + \langle R \rangle^{tr}}{\rho_s y} \\ &+ \frac{\langle R \rangle^{tr} \rho_s V_{30}}{\rho_s y} \\ &= - \frac{V_{30}}{2y} (\langle R \rangle^{hl} - \langle R \rangle^{tr}) \end{aligned} \quad (\text{A13b})$$

as before, assuming no flux across the equator or pole.

In this approximation the high-latitude box is the same as (A13b). The factor of $\frac{1}{2}$ appears in (A13b) because the average advecting velocity in the two-slab approximation is $\frac{1}{2}$ of V_{30} .

We now use equations (A12), (A13b), and (A7) to obtain the two-slab version of (A1).

$$\begin{aligned} \frac{\partial \langle R \rangle^{tr}}{\partial t} &= -W_{tr} \frac{\partial \langle R \rangle^{tr}}{\partial z} - \frac{V_{30}}{2y} (\langle R \rangle^{hl} - \langle R \rangle^{tr}) \\ &+ \frac{K_y (\langle R \rangle^{hl} - \langle R \rangle^{tr})}{y^2} - \langle C \rangle^{tr} \langle R \rangle^{tr} \end{aligned} \quad (\text{A14})$$

$$\begin{aligned} \frac{\partial \langle R \rangle^{hl}}{\partial t} &= +W_{tr} \frac{\partial \langle R \rangle^{hl}}{\partial z} - \frac{V_{30}}{2y} (\langle R \rangle^{hl} - \langle R \rangle^{tr}) \\ &- \frac{K_y (\langle R \rangle^{hl} - \langle R \rangle^{tr})}{y^2} - \langle C \rangle^{hl} \langle R \rangle^{hl} \end{aligned} \quad (\text{A15})$$

Here, self-consistent averages for C are performed in spherical coordinates for the 0–30° (tropical) and 30–90° (high-latitude) boxes.

Since C is nearly independent of R for most all long-lived trace gases, we can once and for all calculate C and its variation with latitude. Thus we write

$$\langle C \rangle^{hl} = b \langle C \rangle^{tr} \quad (\text{A16})$$

From the three-dimensional N₂O model described in this paper we integrate the effective removal coefficient over the sphere from 0–30° and 30–90° to get $b \approx 0.68$. Using (A10) and (A16) we relate $\langle C \rangle^H$ to $\langle C \rangle^{tr}$

$$\langle C \rangle^H = \frac{\langle C \rangle^{tr} + \langle C \rangle^{hl}}{2} = \frac{\langle C \rangle^{tr} + b \langle C \rangle^{tr}}{2} = \frac{(1+b)}{2} \langle C \rangle^{tr} \quad (\text{A17})$$

Now subtract (A14) from (A15), substitute (A16), add an identity, divide by $-y(\partial \langle R \rangle^H / \partial z)$, and assume $\partial / \partial t \langle R \rangle^H = 0$ to get

$$\begin{aligned} \frac{\partial}{\partial t} \frac{[(\langle R \rangle^{hl} - \langle R \rangle^{tr}) / y]}{(-\partial \langle R \rangle^H / \partial z)} &= \frac{-2W_{tr} \{[(\partial \langle R \rangle^{hl} / \partial z) + (\partial \langle R \rangle^{tr} / \partial z)] / 2\}}{y (-\partial \langle R \rangle^H / \partial z)} \\ &- \frac{(2K_y / y^2) (\langle R \rangle^{hl} - \langle R \rangle^{tr}) / y}{(-\partial \langle R \rangle^H / \partial z)} \\ &+ \frac{\langle C \rangle^{tr} (\langle R \rangle^{tr} - b \langle R \rangle^{hl})}{y (-\partial \langle R \rangle^H / \partial z)} \end{aligned} \quad (\text{A18})$$

Rearranging and using (A11) gives

$$\frac{\partial}{\partial t} \frac{\partial z}{\partial y_R} = - \frac{2W_{tr}}{y} - \frac{2K_y}{y^2} \frac{\partial z}{\partial y_R} - \langle C \rangle^{tr} \frac{\partial z}{\partial y_R} - \frac{\langle C \rangle^{tr} (1-b) \langle R \rangle^{hl}}{y (\partial \langle R \rangle^H / \partial z)} \quad (\text{A19})$$

Now eliminate $\langle R \rangle^r$ from (A8) and (A11) to obtain

$$\langle R \rangle^h = \langle R \rangle^r - \frac{y}{2} \frac{\partial \langle R \rangle^h}{\partial z} \frac{\partial z}{\partial y_R} \quad (\text{A20})$$

This is now in terms of globally averaged quantities.

Substitute (A20) into (A19) to get

$$\begin{aligned} \frac{\partial}{\partial t} \frac{\partial z}{\partial y_R} = & -\frac{2W_{tr}}{y} - \frac{2K_y}{y^2} \frac{\partial z}{\partial y_R} - \langle C \rangle^r \frac{\partial z}{\partial y_R} \\ & - \frac{\langle C \rangle^r(1-b)}{y} \frac{\langle R \rangle^h}{(\partial \langle R \rangle^h / \partial z)} + \frac{\langle C \rangle^r(1-b)}{2} \frac{\partial z}{\partial y_R} \end{aligned} \quad (\text{A21})$$

We now set the left-hand side to zero (assuming long-term transport/chemical equilibrium), and solve for $\partial z / \partial y_R$ to obtain

$$\frac{\partial z}{\partial y_R} = -\frac{(2W_{tr}/y) - [(1-b)\langle C \rangle^r/y \partial \ln \langle R \rangle^h / \partial z]}{\partial K_y / y^2 + [(1+b)/2]\langle C \rangle^r} \quad (\text{A22})$$

Before we engage in a more complete analysis, some simple physically useful insights can be gained by inspecting the character of (A22) for the "slow-chemistry limit." That is, the case in which $\langle C \rangle^r \rightarrow 0$. The actual range of applicability will be assessed with the more complete solution of the problem. Near this slow chemistry limit (A22) becomes

$$\frac{\partial z}{\partial y_R} \approx \frac{-W_{tr}}{(K_y/y)} = \frac{\text{Upward advection velocity}}{\text{Meridional diffusion velocity}} \quad (\text{A23})$$

Near this limit the equilibrium tracer slope must appear as a balance between the slope-steepening effect of the vertical diabatic circulation and slope-flattening effect of quasi-horizontal meridional diffusion. This result for the equilibrium tracer slope is essentially the same as that given in the companion treatment of this approach given by *Holton* [this issue]. The more general expression of (A22) differs somewhat from *Holton's* equation (12) mainly because of his implicit assumption that $b \rightarrow 1$ (latitudinally invariant destruction rate).

We now assign values typical for the lower stratosphere. Assume here that the annual mean, 0–30° latitude diabatic heating rate is $\langle Q \rangle^r / c_p \approx 0.3 \times 10^{-5} \text{ deg s}^{-1}$ and that $\partial \langle T \rangle^r / \partial z \ll g / c_p$. (This diabatic heating rate is consistent with those obtained from the annual averages of both the GFDL "Zodiac" and "SKYHI" general circulation models at an altitude near 20 km.) This gives from the thermodynamic equation

$$W_{tr} \approx \frac{\langle Q \rangle^r / c_p}{g / c_p} \approx +0.03 \text{ cm s}^{-1} (\sim 0.8 \text{ km month}^{-1}) \quad (\text{A24})$$

The observed hemispheric mean slope of quasi-conservative tracers in the stratosphere is about -1×10^{-3} [*Machta and Telegadas, 1973*]. Using all of these numbers, we solve for K_y in (A23) to get

$$K_y \approx 1.1 \times 10^{10} \text{ cm}^2 \text{ s}^{-1} \quad (\text{A25})$$

This is a value which is reasonably consistent with independent estimates from a number of empirical two-dimensional transport models. However, this value of K_y and the balance of (A23) are in sharp contrast to several recent two-dimensional model formulations which have argued that meridional diffusion is of secondary importance [*Holton, 1981; Garcia and Solomon, 1983; Tung, 1984*] provided that a "proper" meridional circulation is used (e.g., Lagrangian mean, diabatic, or "residual"). It is also interesting to note that this inferred K_y value of $1.1 \times 10^{10} \text{ cm}^2 \text{ s}^{-1}$ is in the range

identified in the theoretical/modeling study of *R. A. Plumb and J. D. Mahlman* (unpublished manuscript, 1986). They find an effective K_y value of about $2 \times 10^{10} \text{ cm}^2 \text{ s}^{-1}$ in the subtropical anticyclone "surf zone" area and about $0.3 \times 10^{10} \text{ cm}^2 \text{ s}^{-1}$ in mid-latitudes. We note that these values may not be strictly comparable, since the two-slab value of K_y is essentially appropriate for flux across the 30° latitude circle. This is near the poleward edge of the subtropical "surf zone" identified by *R. A. Plumb and J. D. Mahlman* (unpublished manuscript, 1986).

A recent study by *Ko et al. [1985]* on two-dimensional transport modeling in isentropic coordinates suggests a K_y value of about $0.3 \times 10^{10} \text{ cm}^2 \text{ s}^{-1}$. This is more than a factor of 3 lower than that suggested by the above analysis. The explanation for this discrepancy may be due to the local "surf zone" effect mentioned above, the crudity of the two-slab model, or possibly, other factors.

With these preliminary insights gained we now proceed to complete the analysis begun through the derivation of (A22). If the original assertion of section 3 is indeed correct, (A22) can be evaluated directly. That is because the indication was that globally averaged one-dimensional behavior is directly predictable for suitably long-lived, fully equilibrated trace gases (exceptions arising upon violation of these two requirements are given by *Mahlman [1975]*). This assertion implies that the only R dependence in (A22) ($\partial \ln \langle R \rangle^h / \partial z$) can be solved independently of (A22). We now investigate the global properties of the two-slab model to evaluate that assertion.

To produce a fully self-consistent global mean equation, we first combine the mass continuity equation (A2) in log pressure coordinates with (A1) to obtain the flux form tracer continuity equation in the two-slab model (see equation (A13)).

$$\begin{aligned} \rho_s \frac{\partial \langle R \rangle^r}{\partial t} = & -\frac{\partial}{\partial z} \rho_s W_{tr} \langle R \rangle^r - \frac{\rho_s V_{30}}{2y} (\langle R \rangle^h + \langle R \rangle^r) \\ & + (K_y / y^2) (\langle R \rangle^h - \langle R \rangle^r) - \langle C \rangle^r \langle R \rangle^r \end{aligned} \quad (\text{A26})$$

$$\begin{aligned} \rho_s \frac{\partial \langle R \rangle^h}{\partial t} = & +\frac{\partial}{\partial z} \rho_s W_{tr} \langle R \rangle^h + \frac{\rho_s V_{30}}{2y} (\langle R \rangle^h + \langle R \rangle^r) \\ & - (K_y / y^2) (\langle R \rangle^h - \langle R \rangle^r) - b \langle C \rangle^r \langle R \rangle^h \end{aligned} \quad (\text{A27})$$

Here, we have used equations (A7), (A12), and (A16). Now we average (A26) and (A27) to obtain the global average equation

$$\begin{aligned} \rho_s \frac{\partial}{\partial t} \frac{(\langle R \rangle^r + \langle R \rangle^h)}{2} = & +\frac{\partial}{\partial z} \rho_s \frac{W_{tr}}{2} (\langle R \rangle^h - \langle R \rangle^r) \\ & - \frac{\langle C \rangle^r}{2} (\langle R \rangle^r + b \langle R \rangle^h) \end{aligned} \quad (\text{A28})$$

Next, introduce equation (A11) and assume $\partial \langle R \rangle^h / \partial t = 0$ to obtain

$$\begin{aligned} 0 = & -\frac{\partial}{\partial z} \rho_s W_{tr} \frac{y}{2} \frac{\partial z}{\partial y_R} \frac{\partial \langle R \rangle^h}{\partial z} \\ & - \frac{\langle C \rangle^r}{2} \left[(1+b) \langle R \rangle^h + y \frac{\partial z}{\partial y_R} \frac{\partial \langle R \rangle^h}{\partial z} \right] \end{aligned} \quad (\text{A29})$$

We then eliminate $\langle R \rangle^h$, using (A20) to get after some manipulation

$$\begin{aligned} 0 = & -\frac{\partial}{\partial z} \left(\rho_s W_{tr} \frac{y}{2} \frac{\partial z}{\partial y_R} \right) \frac{\partial \langle R \rangle^r}{\partial z} \\ & - \langle C \rangle^r \rho_s \left[\left(\frac{1+b}{2} \right) \langle R \rangle^r + \frac{(1-b)}{4} y \frac{\partial z}{\partial y_R} \frac{\partial \langle R \rangle^r}{\partial z} \right] \end{aligned} \quad (\text{A30})$$

Note that the form of equation (A30) is equivalent to the global average eddy diffusion equation for equilibrium (in log pressure coordinates)

$$\frac{\partial}{\partial z} \rho_s K_z \frac{\partial \langle R \rangle^H}{\partial z} - \rho_s \langle CR \rangle^H = 0 \quad (\text{A31})$$

where from (A30), K_z is defined in the two-slab model by

$$K_z(R) \equiv -\frac{y}{2} W_{tr} \frac{\partial z}{\partial y_R} \quad (\text{A32})$$

Near the "slow-chemistry" limit we get from (A23) and (A32) that $K_z \approx y^2 W_{tr}^2 / 2K_y$. This is very close to the value obtained by Holton's companion analysis [Holton, this issue, equation (14)].

With this we are now in a position to gather a number of insights about the chemistry/transport problem under consideration here. First and easiest, note that the global chemical destruction term in (A30) is already considerably more complex than that traditionally used in one-dimensional models. This is because both C and R vary with latitude. Thus $\langle CR \rangle^H$ depends in (A30) upon $\partial z / \partial y_R$ as well as upon global mean and precomputed quantities (such as b). Further, recall that $\partial z / \partial y_R$ in (A22) can change depending upon the size of the chemical destruction $\langle C \rangle^H$. It is of interest to note that the chemistry term in A30 provides a straightforward approach to parameterization of nonlinear chemical effects in a one-dimensional model.

Most significantly for the present development, (A32) shows that the global one-dimensional diffusion coefficient can change with different trace constituents. This is because $\partial z / \partial y_R$ in (A22) depends upon the efficiency of the chemical destruction. We have yet to determine, however, the relative importance of this effect.

Another useful insight provided by (A32) is a straightforward explanation of the empirical observation that K_z increases with altitude in the upper stratosphere. As stated earlier, W_{tr} depends upon the dynamical forcing of the stratosphere away from a radiative equilibrium state. Because this departure increases notably with altitude, K_z must also do so.

The most important insight to be gained from this analysis is that in general a complete solution of the meridional tracer slope structure and the global mean vertical structure depends upon a mutually consistent solution of equations (A22) and (A30). Thus $\partial z / \partial y_R$ in (A22) depends upon $\langle R \rangle^H$, while $\langle R \rangle^H$ in (A30) depends upon $\partial z / \partial y_R$. Note that this, in principle, refutes both provisional assertions in section 3: (1) that once $\langle R \rangle^H$ is determined for a given tracer with an appropriately determined K_z profile, that profile will work for other long-lived constituents, and (2) all long-lived trace constituents exhibit the same meridional slopes.

We now discuss the methods one might utilize to solve equations (A22) and (A30) for $\partial z / \partial y_R$ and $\langle R \rangle^H$. The most straightforward, of course, is simply to substitute for $\partial z / \partial y_R$ in (A30), using (A22). This operation yields a linear second-order differential equation in $\langle R \rangle^H$ with complicated and variable coefficients. Solving this combined equation for $\langle R \rangle^H$ in turn allows direct determination of $\partial z / \partial y_R$ from (A22).

Because of the direct physical significance of equations (A22) and (A30), greater insight into the relationship between them can be gained by solving them iteratively. A reasonable way to begin is to assume that $\langle C \rangle^H \rightarrow 0$ initially, so that $\partial z / \partial y_R(0)$ is given by (A23). This value is then substituted into (A30), and (A30) is solved for $\langle R \rangle^H(z)$. From this $\partial \ln \langle R \rangle^H / \partial z$ (1) is substituted back into (A22) to get $\partial z / \partial y_R(1)$ and so on.

Since here we are only interested in the degree of coupling between (A22) and (A30), for clarity we seek to simplify the problem. A simple analysis of the square-bracketed term in (A30) shows that the scale height of $\langle R \rangle^H$ has to be smaller than 1.8 km before the second term is within 20% of the magnitude of the first term. Later results indicate that such small-scale heights (large gradients) are to be expected only for extremely rapid removal chemistries. At that limit this simple model becomes inappropriate anyway. Thus we neglect the second term within the square brackets of (A30) to give to an excellent approximation

$$\frac{\partial}{\partial z} \rho_s K_z(R) \frac{\partial \langle R \rangle^H}{\partial z} - \rho_s \langle C \rangle^H \frac{(1+b)}{2} \langle R \rangle^H \approx 0 \quad (\text{A33})$$

where $K_z(R)$ is given by (A32).

Now for analytical convenience we assume that $\rho_s K_z(R) \approx$ constant with height and also that $\rho_s \langle C \rangle^H (1+b/2) \approx$ constant with height. From the lower to the upper stratosphere these are not bad approximations, at least for the present purpose. Under these restrictive assumptions, (A33) has the analytic solution

$$\langle R \rangle^H(z) = \langle R \rangle^H \exp - \left[\frac{(1+b) \langle C \rangle^H}{2 K_z(R)} \right]^{1/2} z' \quad (\text{A34})$$

where $z' = z - z_{\text{trop}}$, and z_{trop} is some "tropopause" height below which $\langle R \rangle^H$ is assumed well mixed and constant. Under these simple conditions, (A34) gives us

$$\frac{\partial \ln \langle R \rangle^H}{\partial z} = - \left[\frac{(1+b) \langle C \rangle^H}{2 K_z(R)} \right]^{1/2} \quad (\text{A35})$$

Substituting (A35) into (A22) yields

$$\frac{\partial y}{\partial y_R} \approx \frac{-W_{tr} + K_z^{1/2} \langle C \rangle^H (1/2 - b/2)^{1/2}}{(K_y/y) + y \langle C \rangle^H (1/2 + b/2)} \quad (\text{A36})$$

We recall here that K_z is dependent upon $\partial z / \partial y_R$, as shown in (A32). The convenient simplification leading to (A34) and (A35) now allows us to evaluate the effect of chemical destruction on the flattening of meridional tracer slopes, with and without " K_z feedback." Here, " K_z feedback" simply means that K_z depends upon $\partial z / \partial y_R$ and that a fully self-consistent calculation must take that into account. However, to clarify the importance of this effect, we solve (A36) in two ways, with and without " K_z feedback."

For the no K_z feedback case, we set K_z at its "slow-chemistry" limit from (A32), using previously obtained values

$$K_z(\text{slow chem}) \approx \frac{-3.6783 \times 10^8 \text{ cm}}{2} \times 0.03 \text{ cm s}^{-2} \\ \times (-1 \times 10^{-3}) \approx 5.5 \times 10^3 \text{ cm}^2 \text{ s}^{-1}$$

This value is close to those used for the region near 20 km in carefully calibrated one-dimensional models [e.g., McElroy *et al.*, 1974; Hunten, 1975]. We now use this value for K_z to solve (A36) for a wide range in values for $\langle C \rangle^H$. For convenience the other values previously established are: $W_{tr} = 0.03 \text{ cm s}^{-1}$; $K_y = 1.1 \times 10^{10} \text{ cm}^2 \text{ s}^{-1}$; $y = 3.6783 \times 10^8 \text{ cm}$, and $b = 0.68$. The slope values obtained are given in the thin-dashed "no K_z feedback" curve in Figure A1. Figure A1 shows that the predicted slope is within 85% of the maximum value (-1×10^{-3}) for local photodestruction times ($1/\langle C \rangle^H$) exceeding ~ 1000 days. However, for $1/\langle C \rangle^H \sim 100$ days, the predicted slope is only about 42% of the "slow-chemistry" value. Thus for chemical destructions of intermediate time scale we already expect a noticeable flattening of the equilibrium slopes. A

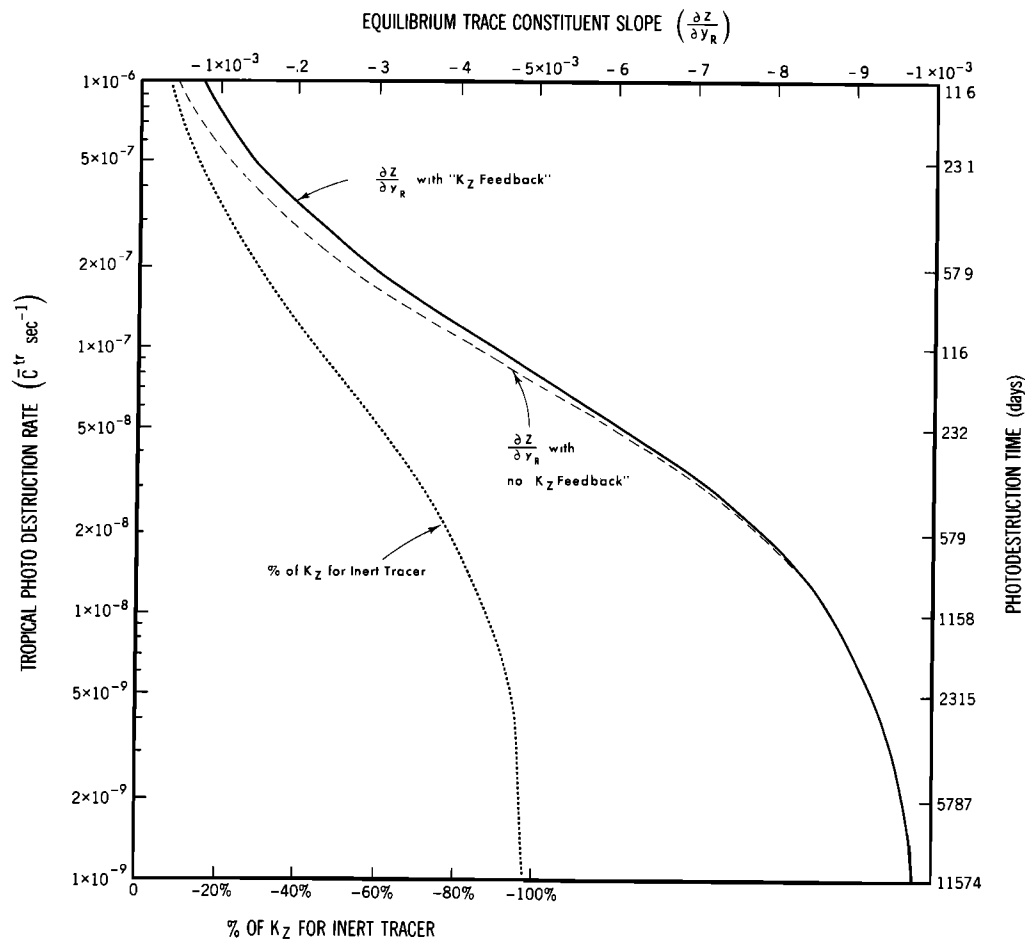


Fig. A1. Two-slab model predictions for effect of chemical destruction on global one-dimensional K_z s and meridional trace constituent slopes. The ordinate is $\langle C \rangle^{\text{tr}}$, the “tropical” mean photodestruction coefficient. The lower abscissa is the percentage reduction of K_z from its “slow-chemistry” limit. The upper abscissa is the equilibrium meridional trace constituent slope.

schematic diagram of these slope-affecting processes is given in Figure A2.

The flattening of these predicted slopes for reasonable chemical destruction time scales implies that K_z (from A32) should also be importantly effected. We next introduce the effect of “ K_z feedback” by substituting (A32) into (A36) and writing the result in the form

$$\begin{aligned} & (\partial z / \partial y_R)^{(n+1)} \\ &= \frac{-W_{\text{tr}} + (-\partial z / \partial y_R)^{1/2(n)} \langle C \rangle^{\text{tr}/2} [y W_{\text{tr}} / (1+b)(1/2 - b/2)]}{(K_z/y) + y \langle C \rangle^{\text{tr}} (1/2 + b/2)} \end{aligned} \quad (\text{A37})$$

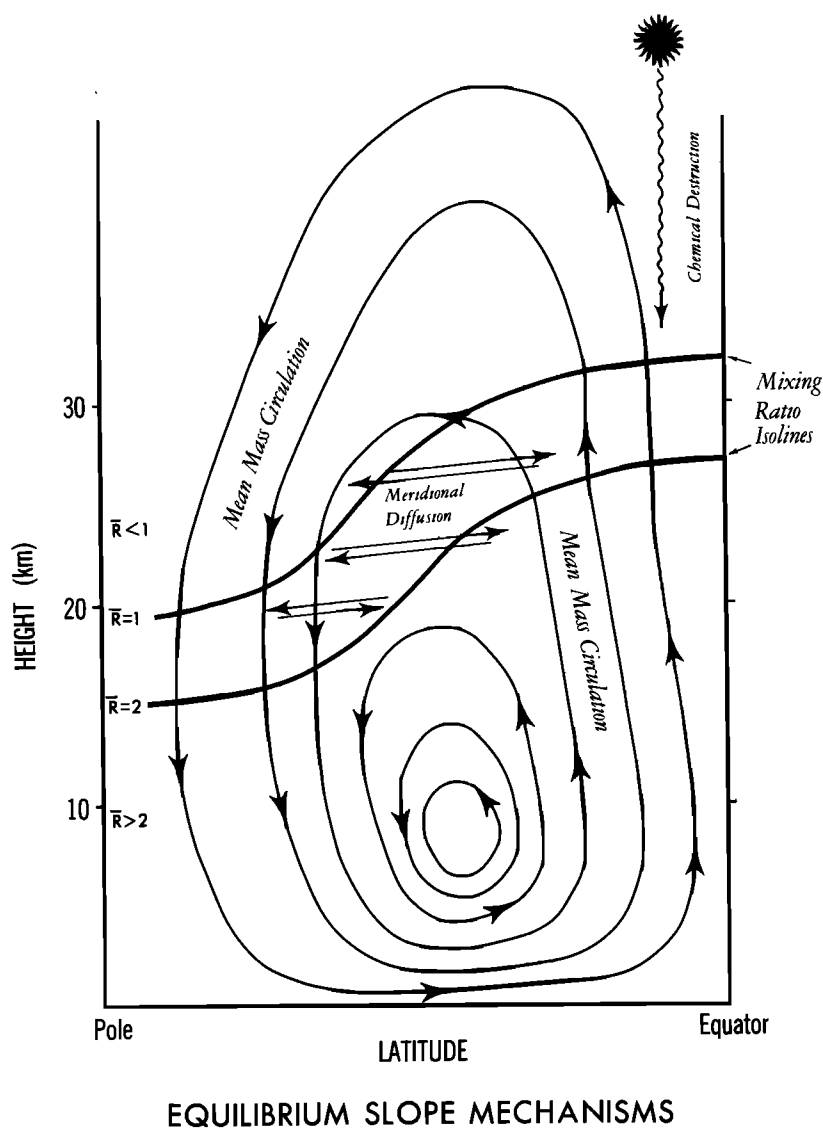
where the n enclosed in superscript braces represents an iteration index. Note that (A37) is formally quadratic in $\partial z / \partial y_R$ and thus could be solved directly. Here, however, we choose to solve (A37) in the indicated iterative manner to maximize our understanding of the effect of “ K_z feedback” on the meridional isoline slopes. This procedure demonstrates that the convergence to the proper solution is very rapid in (A37), typically requiring three or fewer iterations to converge to four-place accuracy. The results for this calculation are given by the heavy solid line in Figure A1. Notice in Figure A1 that the predicted meridional slopes are very similar to that obtained in the “no K_z feedback” limit of (A36).

Thus the meridional slopes of tracer isolines are very depen-

dent upon the chemical destruction rate, but the relative effect of “ K_z feedback” is small except for very fast destruction chemistries. However, the effect of the more complete calculation is to moderate somewhat the slope-flattening effect of the destruction chemistry.

In the companion analysis of Holton [this issue] the second term in the numerator of (A36 or A37) does not appear, by virtue of his assumption that $b \approx 1$. Analysis of the complete solution of (A37) suggests that his simplification of our analysis is indeed reasonable. The largest values of this term occur at high-destruction rates ($\langle C \rangle^{\text{tr}} = 10^{-6} \text{ s}^{-1}$), where it becomes about 12% of W_{tr} . At $\langle C \rangle^{\text{tr}} = 10^{-8} \text{ s}^{-1}$ the term has about a 4% effect. Thus at this level of approximation the $\partial z / \partial y_R$ equation (A37) is effectively decoupled from the K_z equation (A32). Remember, however, that the K_z value is strongly affected by the slope-flattening effect of chemical destruction, as determined by (A37).

The lower scale in Figure A1 shows the dependence of K_z in this two-slab model on the value of the photodestruction coefficient $\langle C \rangle^{\text{tr}}$ (expressed as a percentage of the K_z appropriate for a nearly inert tracer). This shows that the effective K_z in this model becomes much smaller in regions where $\langle C \rangle^{\text{tr}}$ becomes quite large. In this context then, one-dimensional models using a fixed K_z might calculate too much vertical transport of substances in regions characterized by rapid destruction rates. It would be of interest to evaluate this effect in a comprehensive one-dimensional photochemical model to see



EQUILIBRIUM SLOPE MECHANISMS

Fig. A2. Schematic diagram illustrating the three competing processes determining the equilibrium meridional slopes of trace constituent isolines: the slope-steepening effect of the diabatic circulation, and the slope-flattening effects of irreversible meridional diffusion and photochemical destruction.

the model sensitivity to this type of change. This could be readily tested in a one-dimensional model through an iterative coupling of equations (A22) and (A30).

The physical interpretation of this reduced K_z effect is quite straightforward. In the two-slab model, the net vertical flux depends upon (for an "upward" tracer) the tracer amount moving upward in the tropical box being larger than the amount moving downward in the high-latitude box. A reduced slope for a given global mean vertical gradient means a reduced value of meridional gradient ($\langle R \rangle^{\text{tr}} - \langle R \rangle^{\text{hl}}$) (see equation (A28)). It should be noted that this effect could be less in the real atmosphere as a result of the additional presence of local vertical transport events that are somewhat diffusive in character, in contrast to the advective character of the global mean vertical flux in the two-slab model.

Acknowledgments. The authors are grateful to J. Bacmeister, J. R. Holton, R. A. Plumb, J. Sarmiento and an anonymous reviewer for their perceptive comments and suggestions on the work presented here. J. Kennedy, J. Connor, and P. Tunison's group provided valuable technical assistance.

REFERENCES

- Ackerman, M., Ultraviolet solar radiation related to mesospheric processes, in *Mesospheric Models and Related Experiments*, pp. 149–159, D. Reidel, Hingham, Mass., 1971.
- Andrews, D. G., and M. E. McIntyre, Planetary waves in horizontal and vertical shear: The generalized Eliassen-Palm relation and the mean zonal acceleration, *J. Atmos. Sci.*, **33**, 2031–2048, 1976.
- Andrews, D. G., J. D. Mahlman, and R. W. Sinclair, Eliassen-Palm diagnostics of wave, mean-flow interaction in the GFDL "SKYHI" general circulation model, *J. Atmos. Sci.*, **40**, 2768–2784, 1983.
- Breiland, J. G., Comparison of the vertical distribution of thermal stability in the lower stratosphere with the vertical distribution of ozone, *J. Atmos. Sci.*, **24**, 569–576, 1967.
- Breiland, J. G., Some large-scale features of the vertical distribution of atmospheric ozone associated with the thermal structure of the atmosphere, *J. Geophys. Res.*, **73**, 5021–5028, 1968.
- Dobson, G. M. B., The laminated structure of ozone in the atmosphere, *Q. J. R. Meteorol. Soc.*, **99**, 599–607, 1973.
- Dickinson, R. E., Theory of planetary wave-zonal flow interaction, *J. Atmos. Sci.*, **26**, 73–81, 1969.
- Dunkerton, T., On the mean meridional mass motions of the stratosphere and mesosphere, *J. Atmos. Sci.*, **35**, 2325–2333, 1978.
- Ehhalt, D. H., E. P. Roth, and U. Schmidt, On the temporal variance of stratospheric trace gas concentrations, *J. Atmos. Chem.*, **1**, 27–51, 1983.

- Fels, S. B., J. D. Mahlman, M. D. Schwarzkopf, and R. W. Sinclair, Stratospheric sensitivity to perturbations in ozone and carbon dioxide: Radiative and dynamical response, *J. Atmos. Sci.*, **37**, 2265–2297, 1980.
- Frederick, J. E. and J. E. Mentall, Solar irradiance in the stratosphere: Implications for the Herzberg continuum absorption of O₂, *Geophys. Res. Lett.*, **9**, 461–464, 1982.
- Garcia, R. R., and S. Solomon, A numerical model of the zonally averaged dynamical and chemical structure of the middle atmosphere, *J. Geophys. Res.*, **88**, 1379–1400, 1983.
- Goldan, P. D., W. C. Kuster, D. L. Albritton, and A. L. Schmeltekopf, Stratospheric CFCl₃, CF₂I₂, and N₂O height profile measurements at several latitudes, *J. Geophys. Res.*, **86**, 413–423, 1980.
- Hampson, R. F. (Ed.), Chemical kinetic and photochemical data sheets for atmospheric reactions, *FAA Rep. FAA-EE-80-17*, 490 pp., Fed. Aviat. Admin., Washington, D. C., 1980.
- Hess, P. G., and J. R. Holton, The origin of temporal variance in long-lived trace constituents in the summer stratosphere, *J. Atmos. Sci.*, **42**, 1455–1463, 1985.
- Holton, J. R., Wave propagation and transport in the middle atmosphere, *Philos. Trans. R. Soc. London, Ser. A*, **296**, 73–85, 1980.
- Holton, J. R., An advective model for two-dimensional transport of stratospheric trace species, *J. Geophys. Res.*, **86**, 11,989–11,994, 1981.
- Holton, J. R., A dynamically based transport parameterization for one-dimensional photochemical models of the stratosphere, *J. Geophys. Res.*, this issue.
- Hunten, D. M., The philosophy of one-dimensional modeling, Proceedings of the Fourth Conference on the Climatic Impact Assessment Program, *Rep. DOT-TSC-OST-75-38*, pp. 147–155, U.S. Dep. of Transp., Washington, D. C., 1975.
- Jones, R., and J. Pyle, Observations of CH₄ and N₂O by the Nimbus 7 SAMS: A comparison with in situ data and two dimensional model calculations, *J. Geophys. Res.*, **89**, 5263–5279, 1984.
- Junge, C. E., Residence time and variability of tropospheric trace gases, *Tellus*, **26**, 477–488, 1974.
- Ko, M. K. W., K. K. Tung, D. K. Weisenstein, and N. D. Sze, A zonal-mean model of stratospheric tracer transport in isentropic coordinates: Numerical simulations for nitrous oxide and nitric acid, *J. Geophys. Res.*, **90**, 2313–2329, 1985.
- Kurihara, Y., and J. L. Holloway, Jr., Numerical integration of a nine-level global primitive equations model formulated by the box method, *Mon. Weather Rev.*, **95**, 509–530, 1967.
- Levy, H., II, and J. D. Mahlman, Modeling tropospheric N₂O, in *Proceedings of the NATO Advanced Study Institute on Atmospheric Ozone: Its Variations and Human Influences*, edited by A. C. Aikin, pp. 893–907, Federal Aviation Administration, Washington, D. C., 1980.
- Levy, H., II, J. D. Mahlman, and W. J. Moxim, A preliminary report on the numerical simulation of the three-dimensional structure and variability of atmospheric N₂O, *Geophys. Res. Lett.*, **6**, 155–158, 1979.
- Levy, H., II, J. D. Mahlman, and W. J. Moxim, Tropospheric N₂O variability, *J. Geophys. Res.*, **87**, 3061–3080, 1982.
- Levy, H., II, J. D. Mahlman, and W. J. Moxim, Tropospheric ozone: The role of transport, *J. Geophys. Res.*, **90**, 3753–3772, 1985.
- Machta, L., and K. Telegadas, Examples of stratospheric transport, Proceedings of the Second Conference on the Climatic Assessment Program, *Rep. DOT-TSC-OST-73-4*, pp. 47–56, U.S. Dep. of Transp., Washington, D. C., 1973.
- Mahlman, J. D., Some fundamental limitations of simplified transport models as implied by results from a three-dimensional general-circulation tracer model, Proceedings of the Fourth Conference on the Climatic Impact Assessment Program, *Rep. DOT-TSC-OST-75-38*, pp. 132–146, U.S. Dep. of Transp., Washington, D. C., 1975.
- Mahlman, J. D., Mechanistic interpretation of stratospheric tracer transport, *Issues in Atmospheric and Oceanic Modeling, Advances in Geophysics*, vol. 28A, *Climate Dynamics*, edited by B. Saltzman, pp. 301–320, Academic, Orlando, Fla., 1985.
- Mahlman, J. D., and W. J. Moxim, Tracer simulation using a global general circulation model: Results from a mid-latitude instantaneous source experiment, *J. Atmos. Sci.*, **35**, 1340–1374, 1978.
- Mahlman, J. D., and L. J. Umscheid, Dynamics of the middle atmosphere: Successes and Problems of the GFDL “SKYHI” general circulation model, in *Dynamics of the Middle Atmosphere*, edited by J. R. Holton and T. Matsuno, pp. 501–525, Terra Scientific, Tokyo, 1984.
- Mahlman, J. D., H. Levy II, and W. J. Moxim, Three-dimensional tracer structure and behavior as simulated in two ozone-precursor experiments, *J. Atmos. Sci.*, **37**, 655–685, 1980.
- Mahlman, J. D., D. G. Andrews, D. L. Hartmann, T. Matsuno, and R. G. Murgatroyd, Transport of trace constituents in the stratosphere, *Dynamics of the Middle Atmosphere*, edited by J. R. Holton and T. Matsuno, pp. 387–416, Terra Scientific, Tokyo, 1984.
- Manabe, S., and J. D. Mahlman, Simulation of seasonal and inter-hemispheric variations in the stratospheric circulation, *J. Atmos. Sci.*, **33**, 2185–2217, 1976.
- McElroy, M. B., Sources and sinks for nitrous oxide, in *Proceedings of the NATO Advanced Study Institute on Atmospheric Ozone: Its Variations and Human Influences*, edited by A. C. Aikin, p. 345–364, Federal Aviation Administration, Washington, D. C., 1980.
- McElroy, M. B., S. Wofsy, J. Penner, and J. McConnell, Atmospheric ozone: Possible impact of stratospheric aviation, *J. Atmos. Sci.*, **31**, 287–303, 1974.
- Moortgat, G. K., and E. Kudzusz, Mathematical expression for the O(¹D) quantum yields from the O₃ photolysis as a function of temperature (230–320°K) and wavelength (295–320 nm), *Geophys. Res. Lett.*, **5**, 191–194, 1978.
- Plumb, R. A., Eddy fluxes of conservative quantities by small-amplitude waves, *J. Atmos. Sci.*, **36**, 1699–1704, 1979.
- Schemeltekopf, A. L., et al., Stratospheric nitrous oxide profiles at various latitudes, *J. Atmos. Sci.*, **34**, 729–736, 1977.
- Selwyn, G., J. Podolske, and H. S. Johnston, Nitrous oxide ultraviolet absorption spectrum at stratospheric temperatures, *Geophys. Res. Lett.*, **4**, 427–430, 1977.
- Simon, P., Irradiation solar flux measurements between 120 and 400 nm: Current position and future needs, *Planet. Space Sci.*, **26**, 355–365, 1978.
- Tung, K. K., Modeling of tracer transport in the middle atmosphere, *Dynamics of the Middle Atmosphere*, edited by J. R. Holton and T. Matsuno, pp. 417–444, Terra Scientific, Tokyo, 1984.
- Wofsy, S. C., Interactions of CH₄ and CO in the earth's atmosphere, *Annu. Rev. Earth Planet. Sci.*, **4**, 441–469, 1976.

H. Levy II, J. D. Mahlman, and W. J. Moxim, Geophysical Fluid Dynamics Laboratory, Princeton University, P.O. Box 308, Princeton, NJ 08542.

(Received April 22, 1985;
revised November 19, 1985;
accepted November 22, 1985.)